High-Tc Superconducting Bolometer Noise Measurement using Low Noise Transformers - Theory and Optimization

Shahid Aslam, Hollis H Jones
GSFC/NASA, Greenbelt, MD, 20771, USA

Email: *shahid.aslam-1@nasa.gov*

Abstract. Care must always be taken when performing noise measurements on high-Tc superconducting materials to ensure that the results are not from the measurement system itself. One situation likely to occur is with low noise transformers. One of the least understood devices, it provides voltage gain for low impedance inputs (< 100Ω), e.g., YBaCuO and GdBaCuO thin films, with comparatively lower noise levels than other devices for instance field effect and bipolar junction transistors. An essential point made in this paper is that because of the complex relationships between the transformer ports, input impedance variance alters the transformer's transfer function—in particular, the low frequency cutoff shift. The transfer of external and intrinsic transformer noise to the output along with optimization and precautions are treated; all the while, we will cohesively connect the transfer function shift, the load impedance, and the actual noise at the transformer output.

1. Introduction

Complete transformer theory and analysis is widely covered in literature, e.g., Ref. [1]; yet, there is little that also treats noise. This tutorial paper explores the noise generated within the transformer and its relationship to the input and output ports. We examine the transformer as a passive, noise-free network described by an impedance matrix and establish voltage gain relationships between the input and output ports, considering the input source impedance and output load, as well as other relationships [2]. The noise spectral density of the output is then calculated and its connection to other parts of the transformer investigated. Referring the noise to the input by creating equivalent noise sources and the understanding of a simplified noise-generating circuit will illuminate the limits of the noise measurements in terms of source impedance and frequency [3]. From this same circuitry, a commonly used figure of merit—the noise factor—is derived and its advantages are discussed [8]. Finally, we look at the transformer output impedance and its relationship to a subsequent gain device(s), such as a low noise amplifier or a spectrum analyzer, in order to examine the total system noise and the signal-to-noise ratio [13].

2. Transformer Network Analysis

In this work, the transformer is treated as a network in which the internal elements are described mathematically at the input/output ports [2]. The transformer shown in figure 1(*a*) consists of two windings of resistances R_p and R_s with inductances L_p and L_s mutually connected by M—subscripts 'p' and 's' indicate primary and secondary. Mutual inductance is defined as $M \equiv k \cdot \sqrt{L_p \cdot L_s}$, where $0 \le k \le 1$ is the *coefficient of coupling* between the windings. In this work, $k \to 1$ and stray capacitances are neglected. The *turns-ratio* of the *p-s* windings is $n \equiv \sqrt{\frac{L_s}{L_p}} = \frac{V_s}{V_p}$, where V_p and V_s are the voltages across L_p and L_s.

An active or passive device connected to signal source V_g of internal impedance Z_g and to load Z_L at the output can be analyzed as a two-port, *z*-parameter network as depicted in figure 1(*b*). The central larger box represents the transformer circuit of figure 1(*a*) and, for now, is considered noise free. The impedance matrix $\boldsymbol{Z}$ represents elements inside the box such that the voltages and currents at the input and output ports are described by,

$$\mathbf{V} = \mathbf{Z} \cdot \mathbf{I} = \begin{bmatrix} V_1 \\ V_2 \end{bmatrix} = \begin{bmatrix} z_{11} & z_{12} \\ z_{21} & z_{22} \end{bmatrix} \cdot \begin{bmatrix} I_1 \\ I_2 \end{bmatrix} \tag{1}$$

The immittance parameters z_{11} and z_{22} in (1) are the *self-impedances* and z_{12} and z_{21} are the *transfer*-or—for the transformer—*mutual-impedances*. The *z*-parameters are determined by a combination of ratio and open-circuit configurations of the voltages and currents at and into the ports:

$$(a)\quad z_{11} = \left.\frac{V_1}{I_1}\right|_{I_2 = 0} \quad (b)\quad z_{12} = \left.\frac{V_1}{I_2}\right|_{I_1 = 0} \quad (c)\quad z_{21} = \left.\frac{V_2}{I_1}\right|_{I_2 = 0} \quad \text{and} \quad (d)\ z_{22} = \left.\frac{V_2}{I_2}\right|_{I_1 = 0} \tag{2}$$

Applying (2*a*)-(2*d*) to the transformer network gives the following *z*-parameters as functions of $s = j\omega$,

$$(a)\quad z_{11}(s) = R_\mathrm{p} + s \cdot L_\mathrm{p} \qquad (b)\quad z_{12}(s) = z_{21}(s) = s \cdot M \qquad (c)\ \text{and}\quad z_{22}(s) = R_\mathrm{s} + s \cdot L_\mathrm{s} \tag{3}$$

Looking into the k^{th} port with the j^{th} port open ($I_j = 0$) implies $M = 0$; thus impedances z_{kk} are separate series combinations of winding resistances and inductances—$z_{12} = z_{21}$ is found through the Laplace transform of Faraday's Law, $v_k = M \cdot \dfrac{\mathrm{d}i_j}{\mathrm{d}t}$.

Referring to figure 1(*b*), the input and output impedances are determined by looking into the primary winding with signal source V_g and source and load impedances, Z_g and Z_L, respectively. The primary impedance, Z_p, is found by inserting $V_2 = -I_2 \cdot Z_\mathrm{L}$ into (1) and solving for I_2. The secondary impedance, Z_s, is found by setting $V_\mathrm{g} = 0$, substituting $V_1 = -I_1 \cdot Z_\mathrm{g}$ in (1) and solving for I_1. The results are,

$$(a)\quad Z_\mathrm{p}(s) = z_{11}(s) - \frac{z_{12}^2(s)}{z_{22}(s) + Z_\mathrm{L}(s)} \quad \text{and} \quad (b)\quad Z_\mathrm{s}(s) = z_{22}(s) - \frac{z_{12}^2(s)}{z_{11}(s) + Z_\mathrm{g}(s)} \tag{4}$$

Relating this to the transformer by substituting (3*a*)-(3*c*) into (4*a*) and (4*b*) gives,

$$(a)\quad Z_\mathrm{p}(s) = \left(R_\mathrm{p} + s \cdot L_\mathrm{p}\right) - \frac{s^2 \cdot M^2}{\left(R_\mathrm{s} + s \cdot L_\mathrm{s}\right) + Z_\mathrm{L}(s)} \quad \text{and} \quad (b)\quad Z_\mathrm{s}(s) = \left(R_\mathrm{s} + s \cdot L_\mathrm{s}\right) - \frac{s^2 \cdot M^2}{\left(R_\mathrm{p} + s \cdot L_\mathrm{p}\right) + Z_\mathrm{g}(s)} \tag{5}$$

The last terms on the right hand sides of (4*a*) and (4*b*)—or (5*a*) and (5*a*)—are the transformer's *secondary* and *primary reflection impedances*, Z_rs and Z_rp, respectively. The impedance looking into a transformer port equals its self-impedance, z_{kk}, minus the reflected impedance of the other port(s); thus, the primary and secondary impedances are $Z_\mathrm{p} = z_{11} - Z_{rs}$ and $Z_s = z_{22} - Z_\mathrm{rp}$. The reflected impedances have a phase relationship to z_{kk} that increases the magnitude and, depending on termination impedances and frequency, can make up a good portion of the total port impedance.

The transformer network of figure 1(*b*) has two types of voltage gain: the *system voltage gain*, $H(s) = V_2(s)/V_\mathrm{g}(s)$, and the *network voltage gain*, $T(s) = V_2(s)/V_1(s)$. Since Z_g is the internal impedance of the voltage source V_g, $H(s)$ cannot be directly measured. $H(s) \cong T(s)$ can be a good approximation, but when dealing with comparable input impedances, a distinction must be made—references to V_g must involve V_1 in figure 1(*b*). Also, as a passive device, the transformer's impedances and correspondingly the system and network gains are dependent on *termination* impedances Z_g and Z_L.

Considering the two voltage gains under an unloaded condition (i.e., removing Z_L) sets $I_2 = 0$ in (1) yielding $V_1 = z_{11} \cdot I_1$ and $V_2 = z_{21} \cdot I_1$. These give open-circuit expressions for $T(s)$ and $H(s)$,

$$(a)\quad T_\mathrm{o}(s) = \left.\frac{V_2(s)}{V_1(s)}\right|_{I_2 = 0} = \frac{z_{12}(s)}{z_{11}(s)} \quad \text{and} \quad (b)\quad H_\mathrm{o}(s) = \left.\frac{V_2(s)}{V_\mathrm{g}(s)}\right|_{I_2 = 0} = \frac{z_{12}(s)}{z_{11}(s) + Z_\mathrm{g}(s)} \tag{6}$$

Reinserting Z_L and replacing both V_g and Z_g with voltage source V_1, the network voltage gain from (1) is,

$$T(s)=\frac{V_2(s)}{V_1(s)}=\frac{z_{12}(s)\cdot Z_{\mathrm{L}}(s)}{z_{11}(s)\cdot\left(z_{22}(s)+Z_{\mathrm{L}}(s)\right)-z_{12}^2(s)}=T_{\mathrm{o}}(s)\cdot\frac{Z_L(s)}{\left(z_{22}(s)+Z_{\mathrm{L}}(s)\right)-z_{12}(s)\cdot T_{\mathrm{o}}(s)} \tag{7}$$

The substitution of $V_1=V_{\mathrm{g}}\cdot Z_{\mathrm{p}}/(Z_{\mathrm{g}}+Z_{\mathrm{p}})$ into (7) gives the *system transfer function*,

$$H(s)=\frac{V_2(s)}{V_{\mathrm{g}}(s)}=\frac{z_{12}(s)\cdot Z_{\mathrm{L}}(s)}{\left(z_{11}(s)+Z_{\mathrm{g}}(\mathrm{s})\right)\left(z_{22}(s)+Z_{\mathrm{L}}(s)\right)-z_{12}^2(s)}=H_{\mathrm{o}}(s)\cdot\frac{Z_{\mathrm{L}}(s)}{\left(z_{22}(s)+Z_{\mathrm{L}}(s)\right)-z_{12}(s)\cdot H_{\mathrm{o}}(s)} \tag{8}$$

As $|Z_L|\rightarrow\infty$, (7) and (8) approach the open-circuit equations of (6*a*) and (6*b*), respectively. Equation (8) merely adds Z_{g} to z_{11} in (7) making it the special case $T(s)=H(Z_g=0,s)$.

From here on, to simplify matters, Z_{g} is replaced with source resistance R_{g} and Z_{L} is replaced with load resistance R_{L}. Substituting the *z*-parameters of (3*a*)-(3*c*) into (8) results in the system transfer function in terms of the transformer elements,

$$H(R_{\mathrm{g}},s)=\frac{s\cdot M\cdot R_{\mathrm{L}}}{s^2\cdot M^2-\left(R_{\mathrm{g}}+R_{\mathrm{p}}+s\cdot L_{\mathrm{p}}\right)\left(R_{\mathrm{L}}+R_{\mathrm{s}}+s\cdot L_{\mathrm{s}}\right)} \tag{9}$$

Examination of (9) reveals that the shape of the transfer function shifts with R_{g}—that is, there is sensitivity to R_{g}. There is sensitivity to R_{L} as well; however, it is usually constant and typically $R_{\mathrm{L}}>>R_{\mathrm{s}}$. In fact to simplify matters again, occurrences of $R_{\mathrm{L}}+R_{\mathrm{s}}$ terms will be replaced with R_{L} in this work.

Note that (9) can be rearranged into the familiar second-order bandpass statement,

$$H(s)=\frac{a_1\cdot s}{s^2+\left(\frac{\omega_{\mathrm{m}}}{Q}\right)\cdot s+\omega_{\mathrm{m}}^2} \tag{10}$$

where the natural frequency, ω_{m}, and quality factor, Q, (hence bandwidth, $\omega_{\mathrm{B}}=\frac{\omega_m}{Q}$) are functions of R_g.

The coefficients are, $a_1=\frac{R_{\mathrm{L}}\cdot M}{L_{\mathrm{p}}\cdot L_{\mathrm{s}}-M^2}$, $\omega_{\mathrm{B}}(R_{\mathrm{g}})=\frac{\left(R_{\mathrm{g}}+R_{\mathrm{p}}\right)L_{\mathrm{s}}+R_{\mathrm{L}}\cdot L_{\mathrm{p}}}{L_{\mathrm{p}}\cdot L_{\mathrm{s}}-M^2}$, and $\omega_{\mathrm{m}}(R_{\mathrm{g}})=\sqrt{\frac{(R_{\mathrm{g}}+R_{\mathrm{p}})\cdot R_{\mathrm{L}}}{L_{\mathrm{p}}\cdot L_{\mathrm{s}}-M^2}}$.

The magnitude density, $A(R_{\mathrm{g}},\omega)=\left|H(R_{\mathrm{g}},s)\right|_{s=j\omega}$, and the phase angle, $\theta(R_{\mathrm{g}},\omega)=\arg\left[H(R_{\mathrm{g}},s)\right]_{s=j\omega}$, are found to be,

$$A(R_{\mathrm{g}},\omega)=\frac{R_{\mathrm{L}}\cdot M\cdot\omega}{\left[\left(M^2-L_{\mathrm{p}}\cdot L_{\mathrm{s}}\right)^2\cdot\omega^4+\left(2\cdot\left(R_{\mathrm{g}}+R_{\mathrm{p}}\right)R_{\mathrm{L}}\cdot M^2+L_{\mathrm{p}}^2\cdot R_{\mathrm{L}}^2+\left(R_{\mathrm{g}}+R_{\mathrm{p}}\right)^2\cdot L_{\mathrm{s}}^2\right)\omega^2+\left(R_{\mathrm{g}}+R_{\mathrm{p}}\right)^2\cdot R_{\mathrm{L}}^2\right]^{\frac{1}{2}}} \tag{11}$$

and

$$\theta(R_{\mathrm{g}},\omega)=\arctan\left[\frac{\left(M^2-L_{\mathrm{p}}\cdot L_{\mathrm{s}}\right)\cdot\omega^2+\left(R_{\mathrm{g}}+R_{\mathrm{p}}\right)R_{\mathrm{L}}}{\left[L_{\mathrm{p}}\cdot R_{\mathrm{L}}+L_{\mathrm{s}}\cdot\left(R_{\mathrm{g}}+R_{\mathrm{p}}\right)\right]\omega}\right] \tag{12}$$

The relationship for maximum gain, $A_{\max}=\frac{a_1}{\omega_{\mathrm{B}}}$, and the lower 3dB cutoff frequency, $\omega_{\mathrm{L}}=\frac{1}{2}\cdot\left(\sqrt{4\cdot\omega_{\mathrm{m}}^2+\omega_{\mathrm{B}}^2}-\omega_{\mathrm{B}}\right)$, gives,

$$A_{\max}(R_{\mathrm{g}})=\frac{R_{\mathrm{L}}\cdot M}{\left(R_{\mathrm{g}}+R_{\mathrm{p}}\right)L_{\mathrm{s}}+R_{\mathrm{L}}\cdot L_{\mathrm{p}}} \tag{13}$$

and,

$$\omega_{\mathrm{L}}(R_{\mathrm{g}}) = \frac{\left[\left(R_{\mathrm{g}}+R_{\mathrm{p}}\right)^2\cdot L_{\mathrm{s}}^2 + R_{\mathrm{L}}^2\cdot L_{\mathrm{p}}^2 - 2\cdot R_{\mathrm{L}}\cdot\left(R_{\mathrm{g}}+R_{\mathrm{p}}\right)\cdot\left(2\cdot M^2 - 3\cdot L_{\mathrm{s}}\cdot L_{\mathrm{p}}\right)\right]^{\frac{1}{2}} - \left(R_{\mathrm{g}}+R_{\mathrm{p}}\right)L_{\mathrm{s}} + R_{\mathrm{L}}\cdot L_{\mathrm{p}}}{2\cdot\left(L_{\mathrm{s}}\cdot L_{\mathrm{p}} - M^2\right)} \quad (14)$$

The high frequency cutoff is, $\omega_{\mathrm{H}} = \omega_{\mathrm{B}} - \omega_{\mathrm{L}}$; typically, however, $\omega_{\mathrm{H}} \approx \omega_{\mathrm{B}}$.

A low noise transformer model is developed here based on the PARC 1900 low-noise transformer using the 1:1000 ports [4]. The model element values are listed in inset of figure 2—from here on these will be referred to as the "model parameters." The parameters, along with R_{g} and R_{L} values, are inserted into (11) and (12) to give the responses seen in figures 2(*a*) and 2(*b*). The gain is displayed in dB, $A_{\mathrm{dB}} = 20\cdot\log(A)$, and the phase in degrees. Figure 2(*a*) depicts the shift of the frequency response as R_{g} varies. The shift of the upper cutoff frequency is negligible compared to the lower cutoff frequency. Utilizing (14), a linear relationship between R_{g} and lower cutoff frequency, f_{L}, is displayed in figure 3(*a*). The absolute sensitivity of f_{L} to R_{g}, ($S_{R_{\mathrm{g}}}^{f_{\mathrm{L}}} = \frac{R_{\mathrm{g}}}{f_{\mathrm{L}}}\cdot\frac{\partial f_{\mathrm{L}}}{\partial R_{\mathrm{g}}}$), is shown in figure 3(*b*). Extrapolation shows a near-unity sensitivity peak at $R_{\mathrm{g}} = 6.4\Omega$; afterwards, it gradually descends to zero (not shown).

For later discussion, three forms of power gains are defined: *i*) *power gain*, $G_{\mathrm{p}} = \frac{P_2}{P_1}$, *ii*) *available power gain*, $G_{\mathrm{a}} = \frac{P_{2\mathrm{a}}}{P_{1\mathrm{a}}}$, and *iii*) *transducer power gain*, $G_{\mathrm{t}} = \frac{P_2}{P_{1\mathrm{a}}}$ [2]. P_1 is the *primary average power* and P_2 is the *secondary average power* delivered to the load. $P_{1\mathrm{a}}$ is the *primary maximum available average power*—the power extracted through power matching with V_{g} and Z_{g}—and $P_{2\mathrm{a}}$ is the *load maximum available average power*. Conjugate-matched terminations are assumed for $P_{1\mathrm{a}}$ and $P_{2\mathrm{a}}$. The powers P_1, P_2 and $P_{1\mathrm{a}}$ are defined as,

$$(a)\ \ P_1 \equiv |I_1|^2\cdot\mathrm{Re}\left(Z_{\mathrm{p}}\right), \qquad (b)\ \ P_2 \equiv |I_2|^2\cdot\mathrm{Re}\left(Z_{\mathrm{L}}\right), \qquad \text{and}\ (c)\ \ P_{1\mathrm{a}} \equiv \frac{|V_{\mathrm{g}}|^2}{4\cdot\mathrm{Re}\left(Z_{\mathrm{g}}\right)} \quad (15)$$

A Thévenin equivalent network of figure 1(*b*) with Z_{g} terminated into V_{g} defines $P_{2\mathrm{a}}$. Looking back into the open-circuit output, the equivalent voltage is determined by (6*b*) and the equivalent secondary impedance by (4*b*). For series-connected V_{eq} and Z_{eq},

$$(a)\ \ V_{\mathrm{eq}} = \frac{z_{12}}{z_{11}+Z_{\mathrm{g}}}\cdot V_{\mathrm{g}} \quad \text{and} \quad (b)\ \ Z_{\mathrm{eq}} = z_{22} - \frac{z_{12}^2}{z_{11}+Z_{\mathrm{g}}} \quad (16)$$

The secondary's maximum available average power occurs at $Z_{\mathrm{L}} = Z_{\mathrm{eq}}^*$. Applying $Z_{\mathrm{eq}} + Z_{\mathrm{eq}}^* = 2\cdot\mathrm{Re}(Z_{\mathrm{eq}})$ to $|V_{\mathrm{eq}}|^2/(Z_{\mathrm{eq}}+Z_{\mathrm{eq}}^*)$ in (16*a*) and (16*b*), the load's maximum available power is,

$$P_{2\mathrm{a}} \equiv \frac{|z_{12}|^2\cdot|V_{\mathrm{g}}|^2}{4\cdot|z_{11}+Z_{\mathrm{g}}|^2\cdot\mathrm{Re}\left(Z_{\mathrm{eq}}\right)} \quad (17)$$

To facilitate calculating power gains, current gain I_2/I_1 is derived by substituting $V_2 = -I_2\cdot Z_{\mathrm{L}}$ in (1),

$$\frac{I_2}{I_1} \equiv -\frac{z_{12}}{z_{22}+Z_{\mathrm{L}}} \quad (18)$$

which when worked into ratio P_2/P_1 gives the *simple power gain*. The ratio of (17) and (15*c*) yields the *available power gain*. Both power gains are written respectively as,

$$(a)\ G_{\mathrm{p}} = \frac{P_2}{P_1} = \frac{|z_{12}|^2 \cdot \mathrm{Re}(Z_{\mathrm{L}})}{|z_{22} + Z_{\mathrm{L}}|^2 \cdot \mathrm{Re}(Z_{\mathrm{p}})} \quad \text{and} \quad (b)\ G_{\mathrm{a}} = \frac{P_{2\mathrm{a}}}{P_{1\mathrm{a}}} = \frac{|z_{12}|^2 \cdot \mathrm{Re}(Z_{\mathrm{g}})}{|z_{11} + Z_{\mathrm{g}}|^2 \cdot \mathrm{Re}(Z_{\mathrm{s}})} \tag{19}$$

in which Z_{eq} is replaced with Z_{s}. Finally, the *transducer power gain* from the ratio of (15*b*) and (15*c*), the application of (18), and the substitution of $V_{\mathrm{g}} = I_1 \cdot (Z_{\mathrm{g}} + Z_{\mathrm{p}})$ is given by,

$$G_{\mathrm{t}} = \frac{P_2}{P_{1\mathrm{a}}} = \frac{4 \cdot |z_{21}|^2 \cdot \mathrm{Re}(Z_{\mathrm{g}}) \mathrm{Re}(Z_{\mathrm{L}})}{\left|(Z_{\mathrm{g}} + Z_p)(z_{22} + Z_{\mathrm{L}})\right|^2} = \frac{4 \cdot |z_{21}|^2 \cdot \mathrm{Re}(Z_{\mathrm{g}}) \mathrm{Re}(Z_{\mathrm{L}})}{\left|(z_{11} + Z_{\mathrm{g}})(z_{22} + Z_{\mathrm{L}}) - z_{12}^2\right|^2} \tag{20}$$

After substituting (3*a*)-(3*c*) and (5*a*)-(5*b*) into (19*a*) and (19*b*), the power gains as functions of ω and R_{g} are,

$$G_{\mathrm{p}}(\omega) = \frac{R_{\mathrm{L}} \cdot M^2 \cdot \omega^2}{\left(R_{\mathrm{L}} \cdot M^2 + R_{\mathrm{p}} \cdot L_{\mathrm{s}}^2\right)\omega^2 + R_{\mathrm{p}} \cdot R_{\mathrm{L}}^2} \tag{21a}$$

and

$$G_{\mathrm{a}}(R_{\mathrm{g}}, \omega) = \frac{R_{\mathrm{g}} \cdot M^2 \cdot \omega^2}{\left[\left(R_{\mathrm{g}} + R_{\mathrm{p}}\right) M^2 + R_{\mathrm{s}} \cdot L_{\mathrm{p}}^2\right]\omega^2 + R_{\mathrm{s}} \cdot \left(R_{\mathrm{g}} + R_{\mathrm{p}}\right)^2} \tag{21b}$$

followed by substitution of (3*a*)-(3*c*) into the right-hand side of (20) to derive the *transducer power gain*,

$$G_{\mathrm{t}}(R_{\mathrm{g}}, \omega) = \frac{4 \cdot R_{\mathrm{g}} \cdot R_{\mathrm{L}} \cdot M^2 \cdot \omega^2}{\left(M^2 - L_{\mathrm{p}} \cdot L_{\mathrm{s}}\right)^2 \cdot \omega^4 + \left[2 \cdot \left(R_{\mathrm{g}} + R_{\mathrm{p}}\right) R_{\mathrm{L}} \cdot M^2 + R_{\mathrm{L}}^2 \cdot L_{\mathrm{p}}^2 + \left(R_{\mathrm{g}} + R_{\mathrm{p}}\right)^2 \cdot L_s^2\right]\omega^2 + \left(R_{\mathrm{g}} + R_{\mathrm{p}}\right)^2 \cdot R_{\mathrm{L}}^2} \tag{22}$$

Comparison of (22) to (11) reveals the relationship, $G_{\mathrm{t}} = 4 \cdot \left(\frac{R_{\mathrm{g}}}{R_{\mathrm{L}}}\right) \cdot A^2$. Because the transformer is a passive device, i.e., no external power is extracted, power gain equations (21*a*), (21*b*), and (22) are always less than unity.

3. Noise Generation in the Transformer

3.1. Noise definitions

Johnson and Nyquist established the theoretical basis for Brownian-type electrical noise in 1928 [5,6]. Referred to as Johnson, Nyquist, white, thermal, etc., noise, all imply the same thing: *a thermally excited vibration of the charge carriers in a conductor* [3]. Other forms of transformer noise can be considered, e.g., *1/f* or Barkhausen noise [7], but for simplicity, only Johnson noise is examined here.

Although random vibrations give zero average currents in conductors, the instantaneous current fluctuations cause voltage fluctuations across any set of terminals. The *available noise power* in the conductor is,

$$P_{\mathrm{t}} = k_{\mathrm{B}} \cdot T \cdot \Delta f \tag{23}$$

where k_B is the Boltzmann's constant (1.38 X 10^{-23} J·K^{-1}), T is the conductor's absolute temperature in Kelvin, and Δf is the noise bandwidth of the measurement system [3,6]. "Available" implies maximum power measured under conjugate-matched conditions.

Assume a noise source such as the resistance member of element Z_{t} as depicted in figure 4(*a*) in which E_{t} represents the generated noise voltage. Given that Z_{t} is a series equivalent resistance and reactance, $Z_{\mathrm{t}}(\omega) = R_{\mathrm{t}}(\omega) + jX_{\mathrm{t}}(\omega)$, to extract the available power, a conjugate load, $Z_{\mathrm{t}}^*(\omega) = R_{\mathrm{t}}(\omega) - jX_{\mathrm{t}}(\omega)$, is placed at the terminals as in figure 4(*b*). The reactances cancel and the real parts form a voltage divider such that $E_{\mathrm{o}} = E_{\mathrm{t}}/2$, where E_{o} is the voltage measured at the load. The power dissipated at the load, the *available power*, is related to (23) by [6],

$$\frac{E_o^2}{\mathrm{Re}[Z_t(\omega)]} = k_B \cdot T \cdot \Delta f \tag{24}$$

and this leads to an expression for the thermally generated r.m.s. voltage across any impedance element,

$$E_t = \sqrt{4 \cdot k_B \cdot T \cdot \mathrm{Re}(Z) \cdot \Delta f} \tag{25}$$

To discern the independence of the noise bandwidth, both sides of (25) are divided by $\sqrt{\Delta f}$ obtaining the *root normalized noise spectral density* in *volts per unit root hertz* [8],

$$S_t(f) = \sqrt{4 \cdot k_B \cdot T \cdot \mathrm{Re}[Z(f)]} \tag{26}$$

The approximation $\sqrt{4 \cdot k_B \cdot T \cdot R}$ is common; that is, Re(Z) is replaced with resistor R leaving the spectral distribution flat at all frequencies. However, according to (26)—and in practice—the spectral density is only as flat as the real part of the source impedance producing the noise. The spectral density in (26) is usually referred to as *narrow-band* noise (the noise content within a 1Hz interval) and E_t in (25) is referred to as *wide-band* noise (the noise content in rectangular-shaped bandwidth Δf) [3,8].

Now consider an amplifier that measures external noise with transfer function $H(s)$. The noise power content in the interval Δf is not the same as that in the signal transfer bandwidth. The signal power content lies in the frequency span, $B = f_H - f_L$, between the ½ power (or −3dB) points. However, *noise bandwidth* is described by a rectangular power content that is equivalent to the total area under the power gain curve throughout its entire frequency span (0, ∞) divided by its maximum—it is known as the *equivalent noise bandwidth* (ENB) because of the equivalent base x height interval. With the power gain equal to the square-magnitude of the transfer function, recalling (11) and (13), the ENB (or Δf) is defined here as,

$$\Delta f(R_g) = \frac{1}{A_{max}^2(R_g)} \cdot \int_0^\infty A^2(R_g, \omega)\, d\omega \tag{27}$$

The ENB is relative to the −3dB bandwidth, B, except for a few filters such as a Chebyshev or Legendre of orders > 3 where it is larger than B [9]. Applying (27) to a 1st-order lowpass filter reduces it to, $\Delta f = (\pi/2) \cdot f_c$, where f_c is the −3dB cutoff frequency. For a m^{th}-order, a lowpass filter with $m > 1$ gives, $\Delta f = (\pi/2)^{(1/2m)} \cdot f_c$.

To understand the role of (27) in noise amplification, assume resistor R_g is connected to the network input of figure 1(*b*) using inset parameters in figure 2. Although hypothetical, also assume that a true-r.m.s., infinite bandwidth, impedance meter measures the noise voltage at the output shown by the setup in figure 5. With E_t as the thermal noise voltage generated by R_g and its spectral density defined by (26), the r.m.s. output voltage with any given R_g is,

$$e_{no}(R_g) = \sqrt{\int_0^\infty S_t^2(\omega) \cdot A^2(R_g, \omega)\, d\omega} \tag{28}$$

Neglecting reactive elements, if the spectral density is constant with frequency such that $S_t(f) = \sqrt{4 \cdot k_B \cdot T \cdot R_g}$, then (28) is modified to,

$$e_{no}^2(R_g) = 4 \cdot k_B \cdot T \cdot R_g \cdot A_{max}^2(R_g) \cdot \left[\frac{1}{A_{max}^2(R_g)} \cdot \int_0^\infty A^2(R_g, \omega)\, d\omega \right] \tag{29}$$

where (28) is seen in the brackets on the right hand side. Through (29), equation (28) reduces to,

$$e_{no}(R_g) = S_t \cdot A_{max}(R_g) \cdot \sqrt{\Delta f(R_g)} \tag{30}$$

Dividing both sides of (30) by $\sqrt{\Delta f}$ produces the noise voltage spectral density, S_{no}, at the output,

$$S_{no}(R_g) = \frac{e_{no}(R_g)}{\sqrt{\Delta f(R_g)}} = S_t \cdot A_{max}(R_g) \tag{31}$$

3.2. Noise definitions applied to low-noise transformer

Inserting the transformer elements and substituting A_{max} from (13) and the spectral density of (26) into (31) provides the *maximum* output noise spectral density,

$$(a)\quad S_{no\,(max)}(R_g) = \frac{R_L \cdot M \cdot \sqrt{4 \cdot k_B \cdot T \cdot R_g}}{(R_g + R_p) \cdot L_s + R_L \cdot L_p} \quad \text{or,} \quad (b)\quad S_{no\,(max)}(R_g)\Big|_{R_L \to \infty} \approx n \cdot \sqrt{4 \cdot k_B \cdot T \cdot R_g} \tag{32}$$

in which n is the turns-ratio and R_L is removed in (34*b*).

Although equations (29)-(32) are considered ideal and the output noise is calculated by knowledge of the input noise, in actual practice the reverse is calculated: the measured output noise is referred to the input by dividing by the gain. As a function of frequency and R_g, the *referred to input* (RTI) noise spectral density is expressed as,

$$S_{ni}(R_g, \omega) = \frac{S_{no}(R_g)}{A(R_g, \omega)} \tag{33}$$

With the bandpass response of the transformer, the input spectral density S_{ni} will have a U-shaped response—*1/f* noise and other factors have effect on actual measurements, but they are discounted here.

To obtain $S_{no}(R_g,\omega)$, Nyquist's theorem is invoked: the output noise spectral density is dependent on the resistance member of the output impedance. Utilizing (26), the output impedance is the parallel combination of the Z_s given in (5*b*) and Z_L. With $Z_L = R_L$ such that $R_L >> R_s$, the real part $R_o = \mathrm{Re}(Z_o)$ is closely approximated by,

$$R_o(R_g, \omega) \cong \tag{34}$$
$$R_L \cdot \frac{(M^2 - L_p \cdot L_s)^2 \cdot \omega^4 + \left[(R_p + R_g)(2 \cdot R_s + R_L) \cdot M^2 + R_s \cdot R_L \cdot L_p^2 + (R_p + R_g)^2 \cdot L_s^2\right] \omega^2 + R_s \cdot R_L \cdot (R_p + R_g)^2}{(M^2 - L_p \cdot L_s)^2 \cdot \omega^4 + \left[2 \cdot R_L \cdot (R_p + R_g) M^2 + R_L^2 \cdot L_p^2 + (R_p + R_g)^2 \cdot L_s^2\right] \omega^2 + R_L^2 \cdot (R_p + R_g)^2}$$

Substitution of (34) into (26) then gives the output noise voltage spectral density in terms of R_g,

$$S_{no}(R_g, \omega) = \sqrt{4 \cdot k_B \cdot T \cdot R_o(\omega, R_g)} \tag{35}$$

To obtain the input noise voltage spectral density, the placement of noise source E_t in series with the input signal source V_g in figure 1(*b*)—assuming that the remainder of the network is noiseless—gives the solution. Since the individual transformer noise sources are uncorrelated, by superposition, the root-sum-squares of the noise sources can be referred to the input as a single noise source, S_{ni}, stated by (33). Based on model parameters (see inset of figure 2), for decade steps of R_g used in (35), figure 6(*a*) plots the *output noise voltage spectral density* curve family. In figure 6(*b*), the *input noise voltage spectral density* curves are derived by dividing (35) by the gain of (11). The results agree with PSpice simulations.

Note that $R_g = 0\Omega$ does not yield zero output noise; there is always intrinsic noise. For example, at $f =$ 100Hz in figure 6(*b*) with $R_g = 0\Omega$, $S_{ni} = 0.035\mathrm{nV}/\sqrt{\mathrm{Hz}}$. Thus, the thermal noise generated by R_g is mixed with the transformer's noise floor. R_g noise can be somewhat obtained by subtracting in quadrature the spectral density baseline $S_{ni}(R_g = 0, \omega)$ from the $S_{ni}(R_g \neq 0, \omega)$ plots,

$$S_{\mathrm{t}}(R_{\mathrm{g}},\omega)=\sqrt{S_{\mathrm{ni}}(R_{\mathrm{g}},\omega)^2-S_{\mathrm{ni}}(0,\omega)^2} \tag{36}$$

From the results shown in figure 7, although this method corrects for low values, as R_{g} increases, another noise contribution becomes evident—the asymptotically flat "corrected" spectral density regions show this. The spectral density values are compared to the values generated by R_{g} with the relative errors and placed into table 1. It is clear that an extra noise source dominates as R_{g} increases—for example, a 5% error is surpassed before R_{g} = 100Ω; at 1kΩ the error is ~42%! Hence, maintaining as low as possible R_{g}, yet remaining greater than the equivalent resistance (0.074Ω, as calculated from the baseline spectral density) is the proper course.

3.3. Defining intrinsic noise sources

To reiterate, if R_{g} is too low, an intrinsic, baseline noise voltage dominates the measurement; on the other hand, for large R_{g}—although the baseline noise is removed—another noise source dominates. This section describes these intrinsic noise sources as well-placed, independent and equivalent noise sources.

We first look at the network box in figure 1(*b*) without elements V_{g}, Z_{g}, and Z_{L} and treat each port as a connection to a one-port network with an opposite open-circuit port [8]. Through Thévenin's theorem, a noiseless network port responds similar to signal input—except there are two noise voltage generators inserted at both ports as shown in figure 8(*a*). Noise is extracted out of the network box to the external noise sources; the spectral densities of these sources are measured at each port with the opposite port open. To define these, the primary and secondary noise voltage generators E_{p} and E_{s} are added to the voltage vector of (1) yielding the linear equations,

$$(a)\;\; V_1+E_{\mathrm{p}}=z_{11}\cdot I_1+z_{12}\cdot I_2 \quad \text{and} \quad (b)\;\; V_2+E_{\mathrm{s}}=z_{21}\cdot I_1+z_{22}\cdot I_2 \tag{37}$$

E_{p} and E_{s} are partially correlated since they represent different fractions of the same internal noise mechanisms [8].

Now consider the arrangement in figure 8(*b*) where voltage and current noise generators, E_{n} and I_{n}, are placed at only the primary port. To show the relationship of this arrangement to that in figure 8(*a*), the statements derived from (1) for figure 8(*b*) are [8,10],

$$(a)\;\; V=z_{11}\cdot I+z_{12}\cdot I_2 \quad \text{and} \quad (b)\;\; V_2=z_{21}\cdot I+z_{22}\cdot I_2 \tag{38}$$

Examination of figure 8(*b*) shows we have expressions $V=V_1+E_{\mathrm{n}}$ and $I=I_{\mathrm{n}}+I_1$ that when combined into (38*a*) and (38*b*) lead to,

$$(a)\;\; V_1+\left(E_n-z_{11}\cdot I_n\right)=z_{11}\cdot I_1+z_{12}\cdot I_2 \quad \text{and} \quad (b)\;\; V_2-z_{21}\cdot I_{\mathrm{n}}=z_{21}\cdot I_1+z_{22}\cdot I_2 \tag{39}$$

Comparing (39) and (37) reveal that E_{p} and E_{s} are related to E_{n} and I_{n} by,

$$(a)\;\; E_{\mathrm{p}}=E_{\mathrm{n}}-z_{11}\cdot I_{\mathrm{n}} \quad \text{and} \quad (b)\;\; E_{\mathrm{s}}=-z_{21}\cdot I_{\mathrm{n}} \tag{40}$$

Substitution of (3*a*) and (3*b*) into (40*a*) and (40*b*) relates E_{p} and E_{s} to the transformer elements:

$$(a)\;\; E_{\mathrm{p}}(s)=E_{\mathrm{n}}(s)-(R_{\mathrm{p}}+s\cdot L_{\mathrm{p}})\cdot I_{\mathrm{n}}(s) \quad \text{and} \quad (b)\;\; E_{\mathrm{s}}(s)=-s\cdot M\cdot I(s) \tag{41}$$

Since E_{p} and E_{s} of (41) are partially correlated, by (40) E_{n} and I_{n} are also partially correlated; however, to ease calculations, consider E_{n} and I_{n} as totally uncorrelated and adequate to represent the total noise [3,8].

The noise source configurations in figures 8(*a*) and 8(*b*) are both independent of R_{g}, and, if considered, the arrangement of figure 8(*b*) proves more advantageous in analyzing noise. Figure 9 shows the complete equivalent transformer circuit that highlights the topology of the input port signal, V_{g}, and noise sources E_{t}, E_{n}, and I_{n}; the single RTI noise source E_{ni} can replace V_{g} in order to represent to total

input noise seen at the source terminals. A salient point here is that this circuit is independent of the gain and the input impedance of the transformer.

Recalling (7) and (8), the relationship between the system and network gains in figure 9 is given by,

$$|H| = \left|\frac{V_2}{V_g}\right| = \left|T \cdot \frac{Z_p}{Z_p + R_g}\right| \tag{42}$$

The noise voltage E_{no} due to E_i at the input port or due to the RTI source E_{ni} assuming $V_g = 0$, is calculated by,

$$E_{no}^2 = |T|^2 \cdot E_i^2 = |H|^2 \cdot E_{ni}^2 \tag{43}$$

The last two terms are of interest and from this the input port noise is, $E_i^2 = \left(E_t^2 + E_n^2\right)\left|\frac{Z_p}{Z_p + R_g}\right|^2 + I_n^2 \cdot \left|\frac{Z_p \cdot R_g}{Z_p + R_g}\right|^2$. Inserting this into (43) yields the r.m.s.-squared noise at the output,

$$E_{no}^2 = \left(E_t^2 + E_n^2\right)|T|^2 \cdot \left|\frac{Z_p}{Z_p + R_g}\right|^2 + I_n^2 \cdot |T|^2 \cdot \left|\frac{Z_p \cdot R_g}{Z_p + R_g}\right|^2 \tag{44}$$

The RTI noise source then can be derived by (43), i.e., $E_{ni} = E_{no}/|H|$, and by noting the right side of (42) appears inside (44). Then after reduction,

$$E_{ni}^2 = E_t^2 + E_n^2 + I_n^2 \cdot R_g^2 \tag{45}$$

shows that the RTI noise source is independent of system gain, H, and input impedance, Z_p.

E_{ni} is defined by three noise generators: R_g noise voltage, E_t, and two intrinsic noise generators, E_n and I_n. Since E_{ni} and E_t can be established, solving for E_n and I_n is straightforward. Via equations (45) and (25), as $R_g \to 0$, $E_{ni} \to E_n$; or as $R_g \to \infty$, $E_{ni} \to I_n \cdot R_g$. There may be an ideal range of R_g that E_t dominates; however, if E_n and/or I_n are considerably high for all R_g, E_t may not be discerned [8]. Usually one cannot accurately measure the input noise to obtain (45) because of probe disturbances—the noise voltages can only be referred to by the output noise. After converting E_n and I_n to spectral densities, i.e., $S_{En} = E_n \cdot \Delta f^{-\frac{1}{2}}$ and $S_{In} = I_n \cdot \Delta f^{-\frac{1}{2}}$ and applying these to (45), the following using (33) determines S_{En} and S_{In},

$$(a)\quad S_{En}(\omega) = S_{ni}(\omega, R_g)\Big|_{R_g = 0} \quad [\text{V}/\sqrt{\text{Hz}}] \qquad \text{and } (b)\quad S_{In}(\omega) = \frac{S_{ni}(\omega, R_g)}{R_g}\Bigg|_{R_g \to \infty} \quad [\text{A}/\sqrt{\text{Hz}}] \tag{46}$$

Figure 10 displays plots of (46*a*) and (46*b*) using the model parameters from figure 2. The S_{En} curve has a minimum at 0.035nV/√Hz from ~0.5Hz to ~1.3 kHz, whereas above 10Hz, S_{In} is flat at 4.075pA/√Hz. Now with the intrinsic noise sources identified, (36) is modified by procedures (46*a*) and (46*b*),

$$S_t(R_g, \omega) = \sqrt{S_{ni}(R_g, \omega)^2 - \left(S_{En}(\omega)^2 + S_{In}(\omega)^2 \cdot R_g^2\right)} \tag{47}$$

With decade R_g values, equation (47) is plotted in figure 11 using the model parameters. One can readily notice the difference between this family of curves and those of figure 7: the spectral density values on the right side of the graph are equal to the S_t values listed in table 1—all now have 0% error! However, each curve grows unbounded for $f <$ 0.1Hz in figure 11—this is because S_{In} is approximated, losing accuracy as $f \to 0$.

3.4. Closer look at equivalent intrinsic noise sources, E_n and I_n

Starting with (46*a*), S_{ni} is the ratio of (35) and (11), i.e., S_{no}/A. Since (35) contains (34), after setting $R_g = 0$, this reduces to S_{En}, the *equivalent input noise voltage spectral density*,

$$S_{\mathrm{En}}(R_\mathrm{L},\omega)=\frac{\left(4\cdot k_\mathrm{B}\cdot T\cdot\left[\frac{\left(L_\mathrm{p}\cdot L_\mathrm{s}-M^2\right)^2}{R_\mathrm{L}}\cdot\omega^4+\left(R_\mathrm{p}\cdot M^2+R_\mathrm{s}\cdot L_\mathrm{p}^2+\frac{R_\mathrm{p}^2}{R_\mathrm{L}}\cdot L_\mathrm{s}^2\right)\cdot\omega^2+R_\mathrm{s}\cdot R_\mathrm{p}^2\right]\right)^{\frac{1}{2}}}{M\cdot\omega} \tag{48}$$

From (46*b*) we have the same ratio, S_{no}/A, but it is divided by R_g. In the limit as $R_g \to \infty$, we obtain the *equivalent input noise current spectral density*,

$$S_{\mathrm{I_n}}(R_\mathrm{L},\omega)=\frac{\sqrt{4\cdot k_\mathrm{B}\cdot T\cdot\left(\frac{L_\mathrm{s}^2}{R_\mathrm{L}}\cdot\omega^2+R_\mathrm{s}\right)}}{M\cdot\omega} \tag{49}$$

As functions of R_L, (48) and (49) reveal that the load can considerably affect the spectral distribution of E_n and I_n, as seen in figures 12(*a*) and 12(*b*). The dotted flat line at the bottom of figure 12(*a*) is the "ideal" S_{En} in the limit of (48) as $R_L \to \infty$ and the diagonal line in figure 12(*b*) is the "ideal" S_{In} in the limit of (49) as $R_L \to \infty$. It is evident that the loading effect on the input noises must considered when selecting the passband. As a rule derived from the graph—and practice, higher values of R_L result in lower input-related noise content in the interval Δf.

Given R_g and R_L, note that S_{En} and S_{In} are minimum within a mid-range of frequencies in figures 10 and 12. The $S_{En\,(min)}$ is found by taking the square of (48) to derive an equivalent resistance. Setting the derivative to zero and solving leads to,

$$R_{\mathrm{En}}(R_\mathrm{L})=R_\mathrm{p}+R_\mathrm{s}\cdot\left(\frac{L_\mathrm{p}^2}{M^2}\right)+\frac{R_\mathrm{p}^2}{R_\mathrm{L}}\cdot\left(\frac{L_\mathrm{s}^2}{M^2}\right)-2\cdot R_\mathrm{p}\cdot\sqrt{\frac{R_\mathrm{s}}{R_\mathrm{L}}}\cdot\left(1-\frac{L_\mathrm{p}\cdot L_\mathrm{s}}{M^2}\right) \tag{50}$$

Only the first two terms of (50) are usually significant—inserting them into equation (26) gives S_{En}. Typically, $R_L >> R_p^2$, thus one can use $R_{\mathrm{En}} \approx R_\mathrm{p}+\frac{R_\mathrm{s}}{n^2}$ within the mid-range passband range to approximate $S_{En\,(min)}$,

$$S_{\mathrm{En\,(min)}} \cong \sqrt{4\cdot k_\mathrm{B}\cdot T\cdot\left(R_\mathrm{p}+\frac{R_s}{n^2}\right)} \tag{51}$$

The minimum spectral density from noise source I_n is found in the limit of (49) as $f \to \infty$ as seen in figure 12(*b*). This leads to an equivalent resistance of,

$$R_{In} \cong \left(\frac{M^2}{L_\mathrm{s}^2}\right)\cdot R_\mathrm{L}=\frac{R_\mathrm{L}}{n^2} \tag{52}$$

The approximated $S_{In\,(min)}$ becomes,

$$S_{\mathrm{In\,(min)}} \cong \sqrt{4\cdot k_\mathrm{B}\cdot T\cdot\left(\frac{n^2}{R_\mathrm{L}}\right)} \tag{53}$$

At the intersection of (49) and the ideal S_{In} in figure 12(*b*), (53) is reasonable close to (49) with less than −5% error for $f > \frac{\sqrt{R_\mathrm{s}\cdot R_\mathrm{L}}}{2\cdot\pi\cdot L_\mathrm{s}}$. At frequencies below this, one should use the ideal case of (49),

$S_{\mathrm{In}} = \dfrac{\sqrt{4 \cdot k_B \cdot T \cdot R_s}}{2 \cdot \pi \cdot f \cdot M}$, to determine the spot frequency spectral density (the noise content within a unit bandwidth centered at f). For our model parameters, $R_{\mathrm{En}} \approx 0.074\Omega$ and $S_{\mathrm{En(min)}} \approx 0.035\mathrm{nV}/\sqrt{\mathrm{Hz}}$ within ~0.1Hz-1 kHz. Also, $R_{\mathrm{In}} \approx 1\ \mathrm{k}\Omega$ and $S_{\mathrm{In(min)}} \approx 4.074\ \mathrm{pA}/\sqrt{\mathrm{Hz}}$ for $f > 5.15$ Hz.

3.5. Relationship between RTI and intrinsic noise sources in terms of frequency and source resistance.

We now look graphically at the relationship between the RTI noise, E_{ni}, and noise sources E_t, E_n, and I_n as a function of frequency and R_g. After converting all to spectral density, (45) leads to,

$$S_{\mathrm{ni}}(R_g, \omega) = \sqrt{S_t(R_g)^2 + S_{\mathrm{En}}(\omega)^2 + S_{\mathrm{In}}(\omega)^2 \cdot R_g^2} \tag{54}$$

Using the model parameters, (54) is mapped as a function of frequency along with noise levels caused by sources E_t, E_n, and I_n for R_g values of 8.6mΩ, 8.6Ω, and 8.6kΩ in figures 13(*a*), 13(*b*), and 13(*c*).

In figure 13(*a*), as $R_g \to 0$, the spectral density is $S_{\mathrm{ni}} \approx S_{\mathrm{En}}$ for all f. Observe that in this situation S_t as well as $S_{\mathrm{In}} \cdot R_g$ fall well below the S_{En} curve and also note that here as well as elsewhere S_{En} is independent of R_g.

At $R_g = R_n = 8.6\Omega$ in figure 13(*b*), there are three regions in which to consider: *i*) $f < f_a$: $S_{\mathrm{ni}} \approx S_{\mathrm{In}} \cdot R_g$, *ii*) $f_a \geq f \geq f_b$: $S_{\mathrm{ni}} \approx S_t$, and *iii*) $f > f_b$: $S_{\mathrm{ni}} \approx S_{\mathrm{En}}$. Frequencies f_a and f_b locate the points where S_t intersect $S_{\mathrm{In}} \cdot R_g$ and S_{En}, respectively; thus by setting the product of (49) and R_n then (48) equal to $\sqrt{4 \cdot k_B \cdot T \cdot R_n}$ and solving both for ω results in,

$$(a)\ f_a = \frac{1}{2\pi} \cdot \sqrt{\frac{R_L \cdot R_s \cdot R_n}{R_L \cdot M^2 - R_n \cdot L_s^2}} \quad \text{and} \quad (b)\ f_b = \frac{1}{2\pi} \cdot \frac{\sqrt{R_L \cdot \left[\left(R_n - R_p \right) M^2 - R_s \cdot L_p^2 \right]}}{L_p \cdot L_s - M^2} \tag{55}$$

Using the model parameters, $f_a = 0.48$ Hz and $f_b = 42$ kHz. Both S_{En} and S_{In} contributions are well below S_t such that one can state $S_{\mathrm{ni}} = S_t$ with little error. As will be shown later, this R_g value is R_n, the optimum source resistance in the frequency span f_a to f_b. Also note in figure 13(*b*) that the optimum frequency occurs when $S_{\mathrm{En}} = S_{\mathrm{In}} \cdot R_g$. This is denoted by f_n and is equal to the geometric center frequency, $f_n = \sqrt{f_a \cdot f_b}$—in our example, $f_n = 142$ Hz.

Finally, in figure 13(*c*), at $R_g = 8.6\mathrm{k}\Omega$, because of R_g^2 in (54), the $S_{\mathrm{In}} \cdot R_g$ term increases faster than S_t for increasing R_g, making I_n the dominant noise source such that $S_{\mathrm{ni}} \approx S_{\mathrm{In}} \cdot R_g$ for all f.

Changing the abscissa in figure 13(*b*) to source resistance R_g and setting the operating frequency to $f_n = 142$ Hz, the optimal R_g values are depicted in figure 14; there are again three regions of dominance to consider: S_{En} at low values of R_g, $S_{\mathrm{In}} \cdot R_g$ at high values of R_g, and S_t in the middle [8]. Choosing the same intersections from above, these points coincide with R_{En} in (50) for the lower limit of R_g and with R_{In} in (53) for the upper limit. R_n also coincides with the geometric center of the lower and upper limit values, $R_n \approx \sqrt{R_{\mathrm{En}} \cdot R_{\mathrm{In}}}$, a point that coincides with the intersection of S_{En} and $S_{\mathrm{In}} \cdot R_g$. The useful source resistance in figure 14 is $0.074\Omega \leq R_g \leq 1\mathrm{k}\Omega$ at $f_n = 142$ Hz.

3.6. Optimum noise resistance of low-noise transformer

Setting $R_g = R_n$ (or as close as possible) is the concept of *noise matching* and this results in the least possible overall noise power making the *optimum noise resistance* of much interest. Since R_n occurs at the intersection of S_{En} and $S_{\mathrm{In}} \cdot R_g$, then $R_n = S_{\mathrm{En}}/S_{\mathrm{In}} = E_n/I_n$. Substituting in (48) and (49) here leads to R_n as a function of load resistance R_L and frequency—note that it does not depend on T,

$$R_{\mathrm{n}}(R_{\mathrm{L}},\omega)=\left[\frac{\frac{\left(L_{\mathrm{p}}\cdot L_{\mathrm{s}}-M^{2}\right)^{2}}{R_{\mathrm{L}}}\cdot\omega^{4}+\left(R_{\mathrm{p}}\cdot M^{2}+R_{\mathrm{s}}\cdot L_{\mathrm{p}}^{2}+\frac{R_{\mathrm{p}}^{2}}{R_{\mathrm{L}}}\cdot L_{\mathrm{s}}^{2}\right)\cdot\omega^{2}+R_{\mathrm{s}}\cdot R_{\mathrm{p}}^{2}}{\frac{L_{\mathrm{s}}^{2}}{R_{\mathrm{L}}}\cdot\omega^{2}+R_{\mathrm{s}}}\right]^{\frac{1}{2}} \tag{56}$$

Looking back at figures 12(*a*) and 12(*b*), though not influenced by R_{g}, R_{n} is dependent on R_{L}. Using the model parameters, figure 15 maps (56) for various load resistances. The curves reflect the input source resistance that ensures the least noise at a given frequency. As expected, R_{n} increases with R_{L}, but also the plateau shifts right to a higher f_{n} as well as having wider and higher plateau frequency regimes. If R_{L} is removed, R_{n} is a diagonal line in log-log scale throughout the spectrum—then there is not a unique optimum frequency point. There is the appearance then that lower R_{L}—hence lower R_{n}—is indicative of lower noise; however, as shown later, this is not the case.

Through the ratio of (51) and (53), with knowledge of the turns-ratio, winding resistances and load, the plateau value of R_{n} of a 1:*n* turns-ratio transformer can be approximated by,

$$R_{\mathrm{n(mid)}}\approx\frac{1}{n}\cdot\sqrt{R_{\mathrm{L}}\cdot\left(R_{\mathrm{p}}+\frac{R_{\mathrm{s}}}{n^{2}}\right)} \tag{57}$$

Inserting (57) into (56*a*) and (56*b*) under the radical gives the optimum frequency, $f_{\mathrm{n}}=\sqrt{f_{\mathrm{a}}\cdot f_{\mathrm{b}}}$.

4. Noise Figure Analysis

4.1. Noise factor definitions applied to low-noise transformer

The study of noise generation in the above low-noise transformer model indicated that *noise matching* would reduce the intrinsic noise present in signal and source noise measurements; in addition, using the proper optimum frequency regime reduces the amount of noise observed. To utilize the previous analysis would always be tedious thus it is desirable to have a technique to obviate this. From literature, there is a figure of merit known as the *noise factor* that in graph form resolves the optimum noise performance by inspection [11,13]. According to IEEE: *the noise factor of a two-port device is the ratio of the available output noise power per unit bandwidth to the portion of that noise caused by the actual source connected to the input terminals of the device, measured at the standard temperature of 290K* [11]. In equation form, this would read [8],

$$\mathrm{F}=\frac{\text{Total available noise output power}}{\text{Available noise output power arising from source thermal noise}}$$

Put into familiar terms, since this refers to *available power*, figure 1(*b*) is examined in a conjugate matched condition: $Z_{\mathrm{L}}=Z_{\mathrm{s}}^{*}$. Letting P_{noa} be the total available noise power at the output and P_{toa} be the portion at the output due to E_{t}, (19*b*) is used to show that the ratio of the available powers at the input is identical to *F*,

$$F=\frac{P_{\mathrm{noa}}}{P_{\mathrm{toa}}}=\frac{G_{\mathrm{a}}\cdot P_{\mathrm{nia}}}{G_{\mathrm{a}}\cdot P_{\mathrm{ta}}}=\frac{P_{\mathrm{nia}}}{P_{\mathrm{ta}}} \tag{58}$$

where P_{nia} and P_{ta} are the available powers of the RTI noise and that due to $\mathrm{Re}(Z_{\mathrm{g}})$, respectively. If we replace V_{g} in (15*c*) with E_{ni} and use (24) to define E_{t}, (58) develops into,

$$F = \frac{\left[\frac{E_{ni}^2}{4\cdot \mathrm{Re}(Z_g)}\right]}{\left[\frac{E_t^2}{4\cdot \mathrm{Re}(Z_g)}\right]} = \frac{E_{ni}^2}{E_t^2} \tag{59}$$

Incorporating (45) into (59) for E_{ni} yields the usual expression seen for the noise factor [3,12],

$$F = 1 + \frac{E_n^2 + I_n^2 \cdot R_g^2}{E_t^2} \tag{60}$$

Equation (60) covers both frequency and source resistance and it demarcates between intrinsic (E_n and I_n) and thermal (E_t) noise sources; moreover, it reveals that $F - 1$ is the ratio of intrinsic and source noise powers.

Primarily F compares the noise of different systems and does not necessarily indicate optimum noise performance; however, the noise factor is useful in that it not only indicates how close one is to the ideal noiseless network but also the degree that the actual network adds to the noise already present [8]. To aid us, the noise factor can be converted into decibels, $NF = 10 \cdot \log_{10}(F)$, and called the *noise figure*. In this form, an ideal network yields NF = 0 dB. At NF = 10 dB, the noise power due to E_n and/or I_n are 10 times that of E_t, at NF = 20 dB it is 100 times, and so on. At NF = 3dB, source and intrinsic noise levels are equal and, from an engineering point of view, it is futile to make measurements for NF > 3 dB [3]. In practice, the nominal optimal performance is found at $0.5\text{dB} \le NF \le 3\text{dB}$.

A signal-to-noise (SNR) aspect of F is found by multiplying both sides of (60) by the input signal power V_g^2 and power gain A^2 [3,13],

$$F = \frac{\mathrm{SNR}_{in}}{\mathrm{SNR}_{out}} \tag{61}$$

Hence, F measures the decrease in SNR through the network. At NF = 3 dB, SNR_{out} is one-half of SNR_{in}, and at NF = 0.5 dB, SNR_{out} is 89.3% of the SNR_{in}.

The advantage of F is the ability to display it as a contour map. With constant R_L, multiplying both sides of (60) by Δf allows the spectral densities of (46*a*) and (46*b*) or (48) and (49) to define F as a function of frequency and source resistance,

$$F(R_g, \omega) = 1 + \frac{S_{En}^2(\omega) + S_{In}^2(\omega) \cdot R_g^2}{S_t^2(R_g)} \tag{62}$$

where, $S_t(R_g) = \sqrt{4 \cdot k_B \cdot T \cdot R_g}$. Based on the transformer model parameters, figure 16 depicts a contour map of the noise figure of a 1:1000 turns-ratio transformer for R_L = 1GΩ. The contours are essentially the loci of points of constant NF as a function of source resistance and operating frequency [7]. Ideally, one keeps the source resistance and frequency selections inside the 3dB contour. The center point of the contour map, a local minimum, agrees with the above calculations for the optimum noise resistance and frequency, (R_n = 8.6Ω and f_n = 142Hz). The NF map presented here is model-based in that higher-order elements are neglected and it does not account for domain-fluctuations of the core [7], 1/*f* noise, etc. NF contour maps are often derived experimentally, (cf. Ref. [4]); however, figure 16 is adequate for tutorial purposes.

To demonstrate the utility of the NF map, consider a 10 Hz, 1kΩ source resistance connected to the transformer primary input. At these values, several facts can be deduced in figure 16 at, say, $NF \approx 10$ dB: the intrinsic noise power swamps the source noise power by a factor of 10 (in voltage, by √10), the RTI noise is $E_{ni} = E_t \cdot 10^{\frac{NF}{20}} = 12.7\text{nV}/\sqrt{\text{Hz}}$, and the SNR throughput is reduced by 10. The map indicates that, for example, to accurately measure E_t noise at10Hz, the source resistance must be reduced by a factor of 10 to meet noise-matched conditions.

This merits some words though: Noise matching is not power or impedance matching—yet they can

coincide. There is not a direct relationship between R_n and the input impedance Z_p in noise matching as in power matching [3]. Adding resistance in series (or in parallel) to increase (or decrease) the source resistance only introduces another thermal noise source making the situation worse. In all cases, the source resistance should be close as possible to R_n.

To optimize noise matching, taking the derivative of (60) with respect to R_g and setting it to zero obtaining $I_n^2 \cdot R_g^2 - E_n^2 = 0$ leads to, again, the optimum noise resistance, $R_g = R_n = \frac{E_n}{I_n}$. Substitution into (60) results in the *minimum noise factor*,

$$F_{min} = 1 + \frac{E_n \cdot I_n}{2 \cdot k_B \cdot T} \tag{63}$$

After converting to S_{En} and S_{In} via (46*a*) and (46*b*)—or (48) and (49), F_{min} can be expressed as,

$$F_{min}(R_L, \omega) = 1 + \frac{S_{En}(R_L, \omega) \cdot S_{In}(R_L, \omega)}{2 \cdot k_B \cdot T} \tag{64}$$

Note that F_{min} is indirectly affected by R_g since it is subsumed under noise-matching conditions. With our model parameters, (64) is plotted in figure 17 along with R_n for R_L = 1GΩ. $NF_{(min)}$ is minimum in the same frequency regime as the R_n plateau. For instance, at f_n = 142Hz and R_n = 8.56Ω, NF_{min} = 0.074dB, the thermal noise generated by $R_g = R_n$ is E_t = 0.377nV/√Hz, and the RTI noise is E_{ni} = 0.381nV/√Hz. Both intrinsic noise sources are minimum and together make r.m.s. noise voltage, $E_t \cdot \sqrt{10^{\frac{NF}{10}} - 1} = \sqrt{E_n^2 + I_n^2 \cdot R_n^2} = \sqrt{2} \cdot E_n$ = 0.0496nV/√Hz. The factor $\sqrt{2} \cdot E_n$ appears because $E_n = I_n \cdot R_g$ when noise-matched.

Since F_{min} varies with R_L according to (64), S_{En}, S_{In} and R_n are written as functions of both frequency and load resistance. Figure 18 plots (63) using the model parameters. The family of curves reveals that with noise-matched conditions at all frequencies, F_{min} decreases markedly with increasing R_L. Obviously, larger R_L has an advantage in bandwidth below the 3dB line; but on the other hand, driving down R_n by way of a lower R_L reduces the optimum frequency. At the minimum of each curve, the optimum frequency is determined by the geometric center, $f_n = \sqrt{f_a \cdot f_b}$.

Another way to look at F is to bring out an order of E_n, I_n, and R_g each in (60) and incorporate F_{min} of (63) and $R_n = \frac{E_n}{I_n}$ to have,

$$F = 1 + \left(\frac{F_{min} - 1}{2} \right) \cdot \left(\frac{R_n}{R_g} + \frac{R_g}{R_n} \right) \tag{65}$$

where $R_g \neq 0$ [8]. With the presence of F_{min}, (65) gives F at f_n. Substituting (64) into (65) and treating S_{En} and S_{In} strictly as functions of R_L leads to,

$$F\left(\frac{R_g}{R_n}, R_L \right) = 1 + \frac{S_{En}(R_L) \cdot S_{In}(R_L)}{4 \cdot k_B \cdot T} \cdot \left(\frac{R_g}{R_n} + \frac{R_n}{R_g} \right) \tag{66}$$

F is mapped using the ratio R_g/R_n in (66) at different R_L values in figure 19, where the values of R_n and f_n are also dependent on R_L. Because of f_n, the minimum points (R_g/R_n = 1) are equal to the F_{min}.

The values of R_g in which F intersects the 3 dB line in figure 19 are two important points to determine. Setting F = 2 in (65) and rearranging gives a quadratic relationship between parameters R_g, R_n, and F_{min}: $\left(\frac{R_g}{R_n} \right)^2 - \frac{2}{(F_{min} - 1)} \cdot \left(\frac{R_g}{R_n} \right) + 1 = 0$. The solutions of this are the intersection points, which after multiplying by R_n give the inequality statement,

$$R_n \cdot \left(\frac{1}{(F_{min}-1)} - \sqrt{\frac{1}{(F_{min}-1)^2}-1} \right) \le R_g \le R_n \cdot \left(\frac{1}{(F_{min}-1)} + \sqrt{\frac{1}{(F_{min}-1)^2}-1} \right) \tag{67}$$

Thus by (67) R_g is kept between the two boundaries, the source noise is equal to or greater than the intrinsic noise.

In conclusion, looking back at figures 12(*a*) and 12(*b*), although S_{En} is affected by R_L, $S_{En\,(min)}$ is not; but $S_{In\,(min)}$ does change significantly with R_L. However, when $R_g = R_n$ within the plateau interval about f_n, the product of (53) and (57) gives (51)—not a function of R_L; therefore, $S_{In}^2 \cdot R_n^2 = S_{En}^2$ is constant. In short, there seems to be no benefit of a large R_L other than the broader curves under the 3dB line. The apparent advantage of increasing R_L to decrease F_{min} is offset by an increase of the thermal noise of R_g, since it must increase to match R_n anyway.

4.2. Approximations of noise factor in low-noise transformer

We now approximate the above work for the mid-range passband about f_n. We start by substituting (51) and (53) into (45) to give the RTI noise power expression in r.m.s.,

$$E_{ni}^2 \cong 4 \cdot k_B \cdot T \cdot \Delta f \cdot \left(\frac{n^2}{R_L} \cdot R_g^2 + R_g + R_p + \frac{R_s}{n^2} \right) \tag{68}$$

a quadratic equation in R_g scaled by $4 \cdot k_B \cdot T \cdot \Delta f$. On the other hand, at f_n, we can substitute (51) and (53) into (64) to obtain the approximation,

$$F_{min} \cong 1 + 2 \cdot \sqrt{\frac{n^2 \cdot R_p + R_s}{R_L}} \tag{69}$$

Inserting this and (57) into (65) leads to the same result as dividing (68) by E_t^2 from (25),

$$F(R_g) \cong 1 + \frac{n^2 \cdot R_p + R_s}{n^2 \cdot R_g} + \frac{n^2 \cdot R_g}{R_L} \tag{70}$$

Or for large turns-ratio and low source resistance, since usually $R_L >> n^2 \cdot R_g$ one can approximate with simply: $F(R_g) \approx \dfrac{R_g + R_p + \dfrac{R_s}{n^2}}{R_g}$.

4.3. Noise factor of low-noise transformer system with source at different temperature

Everything so far has involved the source resistance at the same temperature as the transformer, but consider now the source at a different temperature. F, then, has to be reworked in order to accommodate two temperatures: T (now reserved for R_g) and T_a (reserved for the ambient temperature). Modifying S_{En} and S_{In} in (48) and (49), as well as S_t of (26), allows (62) to be treated as an expression that accounts for all variables,

$$F_x(R_g, R_L, T, T_a, \omega) = 1 + \frac{S_{En}^2(R_L, T_a, \omega) + S_{In}^2(R_L, T_a, \omega) \cdot R_g^2}{S_t^2(R_g, T)} \tag{71}$$

Equation (71) has been relabeled to F_x to distinguish it from F of equation (62), which is at ambient temperature T_a.

To construct a 2D NF map of (71), three parameters are set constant: T_a = 290K, ambient (room) temperature; R_L = 1GΩ, the load; and, assuming that the passband frequency shifts with R_g such that it straddles f_n, we use approximations (51) and (53) to reduce (71) to an expression that relates it to (70),

$$F_{\mathrm{x}}(R_{\mathrm{g}},T) = 1 + \frac{T_{\mathrm{a}}}{T}\cdot\left(F(R_{\mathrm{g}}) - 1\right) \tag{72}$$

Converted into a noise figure, (72) is plotted in figure 20. With the same constraints, applying (51) and (53) to (64) leads to,

$$F_{\mathrm{min\,x}}(T) = 1 + \frac{T_{\mathrm{a}}}{T}\cdot\left(F_{\mathrm{min}} - 1\right) \tag{73}$$

where $F_{\mathrm{min}} - 1$ is taken from (69). Note that figure 20 indicates that the best performance is achieved when the choices of R_{g} and T satisfy the contours above 3dB.

A thermistor-transformer example is now presented in which R_{g} and its temperature T are the only variables, i.e., the transformer temperature, $T_{\mathrm{a}} = 290\mathrm{K}$, remains constant. Using the model parameters, the results are placed into table 2. Included with the variables, F_{x} from (72) and $F_{\mathrm{min\,x}}$ from (73) are also shown. The source spectral density S_{t} is given and, after rearranging (71), the RTI spectral density, $S_{\mathrm{ni\,x}}$, and the S_{En} and S_{In} contributions, $S_{\mathrm{A\,x}}$, are also given. At $T = T_{\mathrm{a}}$ in table 2 (1st row), the temperatures cancel in (72), which, after making $R_{\mathrm{g}} = 30\Omega$, (62) gives the noise factor. The 2nd row sets $R_{\mathrm{g}} = 3\Omega$ at 77K, where the noise factors are well below 2 with a large difference between S_{t} and S_{Ax}. The last row sets $R_{\mathrm{g}} = 0.3\Omega$ at 40K and shows that the noise factor go up as well as the relative difference between S_{t} and S_{nix}; the performance becomes worse because $R_{\mathrm{g}} << R_{\mathrm{n}}$.

$1/F_{\mathrm{x}}$ gives the fractional presence of S_{t} in the total noise S_{ni}. At $T = 290\mathrm{K}$ and $R_{\mathrm{g}} = 30\Omega$, 98% of the total noise is source or R_{g} noise; at $T = 77\mathrm{K}$ and $R_{\mathrm{g}} = 3\Omega$, it is 90.6% of the total noise; and, for $T = 40\mathrm{K}$ and $R_{\mathrm{g}} = 0.3\Omega$, 35.8% of the total is R_{g} noise.

5. DC-blocking Capacitor and Noise Measurement

Some cases require a d.c. blocking capacitor between the source and transformer primary to prevent core magnetization due to bias current; this, however, may have an undesirable effect on the transfer function and noise level. The insertion of a d.c. blocking capacitor into figure 9 is redrawn in figure 21. The capacitor in series with R_{g} forms input impedance $Z_{\mathrm{g}}(\omega) = R_{\mathrm{g}} - jX_{\mathrm{g}}(\omega)$, where $X_{\mathrm{g}}(\omega) = 1/(\omega C_g)$ is the reactance. The substitution of R_{g} for impedance Z_{g} in (45) yields,

$$E_{\mathrm{ni}}^2 = E_{\mathrm{t}}^2 + E_{\mathrm{n}}^2 + I_{\mathrm{n}}^2\cdot\left|Z_{\mathrm{g}}\right|^2 = E_{\mathrm{t}}^2 + E_{\mathrm{n}}^2 + I_{\mathrm{n}}^2\cdot R_{\mathrm{g}}^2 + I_{\mathrm{n}}^2\cdot X_{\mathrm{g}}^2 \tag{74}$$

The additional term signifies extra noise voltage across the capacitor due to I_{n}; moreover, it is frequency dependent due to both I_{n} and X_{g}. This noise has a distinct $1/f$ distribution (not excess noise) and its contribution is inversely proportional to C_{g}.

To lower the cutoff frequency as well as reduce the noise contribution, use as large of C_{g} as possible. With the above transformer model's unusual low cutoff frequency, finding a large value capacitor that does not introduce other unwanted factors is difficult. Electrolytic capacitors, popular for large values, are known for both low accuracy and temperature stability [14]; however, they contribute noise due to leakage currents and should be avoided [12]. *Double layer* capacitors are currently a better choice: They have slightly better accuracy and stability and, with higher series resistance, the leakage is much less [14].

Consider, say, $C_{\mathrm{g}} = 15\mathrm{mF}$ and its effect on the transfer function. Inserting $Z_{\mathrm{g}}(s) = R_{\mathrm{g}} + 1/(s\cdot C)$ into (8) produces figure 22, where only frequencies below 1kHz are shown—higher frequency results are similar to Figure 2(*a*). The plots for $R_{\mathrm{g}} < 10\Omega$ reveal peaking centered at $\frac{1}{2\cdot\pi\cdot\sqrt{L_{\mathrm{p}}\cdot C_{\mathrm{g}}}} \approx 3.15\mathrm{Hz}$ and cutoff frequencies insensitive to R_{g}, e.g., $f_{\mathrm{L}} \approx 2\mathrm{Hz}$. By comparison, the cutoff frequencies in figure 22 are relatively the same as figure 2(*a*) for $R_{\mathrm{g}} \geq 10\Omega$. Also, the curve's ENB is quite different from those of figure 2(*a*), e.g., at $f < 1\mathrm{kHz}$, the ENB is larger for $R_{\mathrm{g}} \leq 1\Omega$ plots.

Substituting $R_{\mathrm{g}} + 1/s\cdot C_{\mathrm{g}}$ into $Z_{\mathrm{g}}(s)$ in (5*b*) with R_{L} in parallel gives R_{o}, which when placed into (35) yields the output spectral densities of figure 23(*a*). In contrast to figure 6(*a*), there is obvious peaking of

the output noise. Divided then by the corresponding amplitudes (figure 22), the family input spectral density curves are given in figure 23(*b*). Comparing figure 23(*b*) to figure 6(*b*), the converging noise values are larger as $f \to 0$ for all R_g. This is due to the noise across X_g and can be compensated by applying (36) to figure 23(*b*) for results similar to figure 7.

Applying the techniques given in (46*a*) and (46*b*) is tantamount to either shorting the left side of C_g in figure 21 to ground to derive S_{En} or setting R_g to a large value (e.g. 1GΩ) to determine S_{In}. Afterwards, applying (47) yields results similar to figure 11. Using S_{En} and S_{In} with (74) and modifying (62) to include C_g leads to,

$$F(R_g,\omega) = 1 + \frac{S_{En}^2(\omega) + S_{In}^2(\omega)\cdot\left(R_g^2 + \dfrac{1}{\omega^2\cdot C_g^2}\right)}{S_t^2(R_g)} \tag{75}$$

From (75), a NF map for our transformer model with C_g = 2.3F along with the inset parameters from figure 2 is displayed in figure 24. Compared to figure 16, the contours on the lower left half of the map shift right in response to the extra capacitance. This is expected since the bandwidth is narrower and there is extra noise power due to X_g. Despite this, R_n and f_n undergo very little change in this example.

6. The Amplifier Chain and Noise

6.1. Secondary resistance without load

The cascade arrangement of the low-noise transformer and amplifiers and/or meter devices is examined in this section. These extra devices generate additional noise that propagates through the system; hence, their noise resistances should be matched—or closely matched. In most cases though, the applied or input noise is already greater than the device's intrinsic noise by a factor of √2. Ideally, all connected stages—whether a transformer or an amplifier/meter—should operate at noise resistance or R_n input conditions and its output resistance should be matched to the following stage's R_n.

With that said, before examining other devices, we isolate first the transformer's output resistance member. Removing R_L and evaluating (5*b*) gives,

$$R_{os}(R_g,\omega) = \frac{\left[\left(R_g + R_p\right)\cdot M^2 + R_s\cdot L_p^2\right]\omega^2 + R_s\cdot\left(R_g + R_p\right)}{L_p^2\cdot\omega^2 + \left(R_g + R_p\right)^2} \tag{76}$$

Figure 25 plots (76) for decade values of R_g using the model parameters. Notice that R_{os} increases whereas f_L shifts to the right with larger R_g; otherwise, the family of curves is flat in the optimum frequency regime and approximated by,

$$R_{os}(R_g) = R_s + n^2\cdot\left(R_g + R_p\right) \tag{77}$$

Equations (76) or (77) are useful for noise matching whereas equation (34), by using R_L, derives the total resistance R_o—eventually, both sets of equations use (35) to obtain S_{no}.

Although meant for transformers, figure 9 serves as a schematic as well for a low-noise amplifier (LNA) or a meter, such as a spectrum analyzer (S/A). The transformer, LNA, and S/A thus use similar equations: (45) for E_{ni}; (46*a*) and (46*b*) for S_{En} and S_{In}; and (62), (64), and (67) for F, $F_{(min)}$ and the R_g boundaries, respectively. For a LNA or S/A, R_g in figure 9 is substituted by the preceding stage drive resistance, e.g., the transformer's output resistance. In the same way, the load resistance, R_L, of a transformer can be the input resistance member of a BJT base or FET gate impedance.

6.2. Cascade power gain, noise power, and noise factors

When comparing systems it is more convenient to evaluate the system gain and noise factor of the entire chain as a single network rather than in piecemeal. Because the individual noise powers are uncorrelated, the derivation of the system noise factor is not as straightforward as the system signal power gain. H. T. Friis, in 1944, was the first to describe a method that evaluates a power transfer system in terms of individual power gains and noise factors [13]. The method also accounts for terminal impedance mismatch; yet the load impedance and input/output resistance thermal noise are of no consequence [8,13].

Figure 26 presents a cascaded power transfer system consisting of three stages: A low-noise transformer of gain A_1 and noise factor F_1; a LNA of A_2 and F_2; and a S/A of A_3 and F_3. Also shown are the intrinsic noise voltage sources, E_{nA_k}, of each k^{th} stage that through (45) are represented by $E^2_{\mathrm{nA}_k} = E^2_{\mathrm{n}_k} + I^2_{\mathrm{n}_k} \cdot R^2_{o_{(k-1)}}$ in which $R_{\mathrm{o}_{(k-1)}}$ is the previous stage's output resistance. The available power gain, G_{a}, is a function of the network z-parameters and source impedance; yet, looking at (19*b*), G_{a} is independent of the load. Combining the magnitude-square of (6*b*) into (19*b*) simplifies G_{a} for each k^{th} stage to,

$$G_{\mathrm{a}_k} = A^2_k \cdot \left(\frac{R_{\mathrm{o}_{(k-1)}}}{R_{\mathrm{o}_k}} \right) \tag{78}$$

where A_{k} is the voltage gain and R_{o_k} is the output resistance of the k^{th} stage, respectively. For k = 1, $R_{\mathrm{o}_0} = R_{\mathrm{g}}$ and $R_{\mathrm{o}_1} = R_{\mathrm{os}}$, according to (77). Evaluating (78) for the transformer and the LNA in figure 26 gives the following results:

$$(a)\;\; G_{\mathrm{a}_1} \approx \frac{n^2 \cdot R_{\mathrm{g}}}{R_{\mathrm{s}} + n^2 \cdot \left(R_{\mathrm{g}} + R_{\mathrm{p}}\right)} = n^2 \cdot \left(\frac{R_{\mathrm{g}}}{R_{\mathrm{os}}} \right) \quad \text{and} \quad (b)\;\; G_{\mathrm{a}_2} \approx \frac{R_{\mathrm{os}} \cdot R^2_{i_2} \cdot A^2_{\mathrm{amp}}}{R_{\mathrm{o}_2} \cdot \left(R_{\mathrm{os}} + R_{\mathrm{i}_2}\right)^2} \approx A^2_{\mathrm{LNA}} \cdot \left(\frac{R_{\mathrm{os}}}{R_{\mathrm{o}_2}} \right) \tag{79}$$

where (79*a*) is the mid-band approximation of (21*b*) and though not shown it is a function of R_{g}. In (79*b*) $A_2 = A_{\mathrm{LNA}} \cdot \frac{R_{\mathrm{i}_2}}{R_{\mathrm{os}} + R_{\mathrm{i}_2}}$, where A_{LNA} is the LNA voltage gain setting; the optimal case, $R_{\mathrm{i}_2} >> R_{\mathrm{os}}$, is assumed for the right-most approximation in (79*b*). For the S/A, the gain is simply set to unity or $G_{\mathrm{a}_3} = 1$.

The total power gain of any measurement system with N gain/attenuator elements is the product of the individual power gains,

$$G_{\mathrm{sys}} = \prod_{k=1}^{N} G_{\mathrm{a}_k} = G_{\mathrm{a}_1} \cdot G_{\mathrm{a}_2} \cdots G_{\mathrm{a}_N} \tag{80}$$

The application of (80) to equations (79*a*), (79*b*), and the S/A gain results in the mid-band approximation of the system in figure 26,

$$G_{\mathrm{sys}}(R_{\mathrm{g}}) \approx n^2 \cdot A^2_{\mathrm{LNA}} \cdot \left(\frac{R_{\mathrm{g}}}{R_{\mathrm{o}_2}} \right) \tag{81}$$

Setting R_{g} constant in figure 26 as well as removing E_{t} and E_{nA_k} noise sources, the input and output available powers are simply $P_{\mathrm{g}} = V^2_{\mathrm{g}} / 4 \cdot R_{\mathrm{g}}$ and $P_{\mathrm{o}} = P_{\mathrm{g}} \cdot G_{\mathrm{sys}}$, respectively. Now if E_{t} is reinstated and P_{g} = 0, (80) gives the power transfer of external noise P_{t} from (23) such that, $P_{\mathrm{no}} = P_{\mathrm{t}} \cdot G_{\mathrm{sys}}$. Figure 27 details the total power transfer through figure 26 after reestablishing noise sources E_{nA_k}. With F_{k} as the individual noise factors, the intrinsic noise power at each k^{th} stage is,

$$P_{\mathrm{nA}_k} = k_{\mathrm{B}} \cdot T \cdot \Delta f \cdot \left(F_k - 1\right) \tag{82}$$

With all parameters constant, (82) depends on resistance only through F_{k}. Setting signal P_{g} = 0 in figure 27, the individual output powers are $P_{\mathrm{no}_1} = G_{\mathrm{a}_1} \cdot k_{\mathrm{B}} \cdot T \cdot \Delta f \cdot F_1$, $P_{\mathrm{no}_2} = G_{\mathrm{a}_2} \cdot [P_{\mathrm{no}_1} + k_{\mathrm{B}} \cdot T \cdot \Delta f \cdot (F_2 - 1)]$, and $P_{\mathrm{no}} = P_{\mathrm{no}_3} = G_{\mathrm{a}_3} \cdot [P_{\mathrm{no}_2} + k_{\mathrm{B}} \cdot T \cdot \Delta f \cdot (F_3 - 1)]$, where $k_{\mathrm{B}} \cdot T \cdot \Delta f$ is the noise power of each source resistance.

Expanding P_{no} results in the total noise power output:

$$P_{no} = k_B \cdot T \cdot \Delta f \cdot G_{sys} \cdot \left(F_1 + \frac{F_2 - 1}{G_{a_1}} + \frac{F_3 - 1}{G_{a_1} \cdot G_{a_2}} \right) \tag{83}$$

From (58) with $P_{toa} = k_B \cdot T \cdot \Delta f \cdot G_{sys}$, the system noise factor is the enclosed terms in (83) and can be further generalized as,

$$F_{sys} = F_1 + \frac{F_2 - 1}{G_{a_1}} + \frac{F_3 - 1}{G_{a_1} \cdot G_{a_2}} + \ldots + \frac{F_N - 1}{G_{a_1} \cdot G_{a_2} \cdots G_{a_{N-1}}} = F_1 + \sum_{i=1}^{N-1} \frac{F_{(i+1)} - 1}{\prod_{n=1}^{i} G_n} \tag{84}$$

Known as *Friis' formula*, (84) is a canonical statement for N gain/attenuator elements in a power transfer system [8,13]. For an optimal system, typically only the first two terms are significant; however, the best performance is obtained when F_1 has significantly more influence over the summation term in (84) [3,8].

6.3. SNR and conversion of cascade transformer/amplifier/meter system

The system of figure 27 can be reduced to the simple power transfer network shown in figure 28. Three input ports represent the system intrinsic and source resistance noise powers with the bottom port for the signal power. P_{out}, the power transfer output, contains both the signal output power, $P_o = P_g \cdot G_{sys}$, and the output noise power now defined as, $P_{no} = P_t \cdot G_{sys} \cdot F_{sys}$. Equations (82) and (84) furnish the system equivalent intrinsic noise power,

$$P_{nA} = k_B \cdot T \cdot \Delta f \cdot \left(F_{sys} - 1 \right) \tag{85}$$

Once G_{sys}, F_{sys}, and the system *ENB* are determined, (58) can be used to determine the SNR using the available power. Applying definitions $SNR_{out} = P_o/P_{no}$, $SNR_{in} = P_g/P_{ni}$, and the above work to (61) leads to,

$$SNR_{out} = \frac{P_g}{k_B \cdot T \cdot \Delta f \cdot F_{sys}} \tag{86}$$

To maintain $SNR_{out} \geq 1$, $P_g \geq k_B \cdot T \cdot \Delta f \cdot F_{sys}$; signal V_g then must be greater than or equal to the system RTI noise voltage,

$$V_g \geq E_{ni} = \sqrt{4 \cdot k_B \cdot T \cdot \Delta f \cdot R_g \cdot F_{sys}} \tag{87}$$

We convert to spectral density by examining figure 29, it is similar to figure 9, except E_{nA} replaces E_{ni} and $I_n \cdot R_g$ and there is not a load impedance. Dividing (87) by $\sqrt{\Delta f}$ gives the system noise voltage spectral density of the equivalent input noise source for a low noise transformer-driven system affected by R_g,

$$S_{ni}(R_g, \omega) = \sqrt{4 \cdot k_B \cdot T \cdot R_g \cdot F_{sys}(R_g, \omega)} \tag{88}$$

Under the same conditions, since P_{nA} of (85) is dependent on R_g via F_{sys}, the system intrinsic noise voltage source is,

$$S_{nA}(R_g, \omega) = \sqrt{4 \cdot k_B \cdot T \cdot R_g \cdot \left(F_{sys}(R_g, \omega) - 1 \right)} \tag{89}$$

To obtain the thermal noise S_t of (26), if A_{sys} and F_{sys} are known at $V_g = 0$, A_{sys} is divided into measurement S_{no} yielding (88), i.e., $S_{ni} = S_{no}/A_{sys}$. Rearranging for S_t then gives,

$$S_t(R_g,\omega) = \frac{S_{no}(R_g,\omega)}{A_{sys}(R_g,\omega)\cdot\sqrt{F_{sys}(R_g,\omega)}} \tag{90}$$

Strictly as a real-number process between zero and one, multiplying S_{no} over A_{sys} by the conversion and correction factor in (90), $F_{sys}^{-\frac{1}{2}}$, gives the noise voltage spectral density of the sensor.

7. Conclusion

One of the underlying themes of this work has been the effect on a low-noise transformer due to variable input source or sensor resistance, R_g. Two concerns were: *i*) a transfer function *highly* dependent upon input/output impedances; the output impedance, however, is usually constant. And *ii*), noise characteristics are determined by source and load impedances; that is, the spectral density distribution is shaped by the transfer function and the magnitude levels depend on termination impedances. We discerned, also, between the two transfer functions: $T(s)$, the *network* gain that is independent of R_g, and $H(s)$, the *system* transfer function that is dependent on R_g. Then we demonstrated with $H(s)$ that the lower frequency cutoff shifts with respect to the sensor or source resistance, R_g.

Nyquist's theorem was applied to acquire the low noise transformer's output noise voltage spectral density; this divided by the gain gave the RTI noise voltage spectral density. It was demonstrated that the magnitude of the noise varies with R_g. Further calculations, where the $R_g = 0\Omega$ baseline was subtracted in quadrature from the $R_g \neq 0\Omega$ curves, revealed that the noise magnitudes changed disproportional to R_g, indicative of intrinsic noises other than the input sensor noise. Two-port analysis defined intrinsic equivalent voltage and current noise sources, E_n and I_n, at the input, which when added in quadrature to the sensor thermal noise gave the correct expression for the RTI noise. The spectral densities for E_n and I_n are derived by zero/high resistance measurement techniques or by calculation. For post-processing, (47) and (27) can be utilized to derive the correct sensor r.m.s. noise, E_t. Equation (54) was mapped at various R_g values to show the advantage of matching the source to R_n, the optimum noise resistance. The optimum frequency, f_n, is the geometric center of endpoints where $S_t = S_{En} = S_{In}\cdot R_g$ —at the center point, $R_g = R_n$. Operating beyond the endpoints allows S_{En} or $S_{In}\cdot R_g$ to dominate S_t. We also looked at the nexus between R_n and R_L; as a note, although not mentioned in above, for large R_L, R_n is on the order of $\sqrt{R_L}/n$.

The *noise factor* (and *noise figure*) absorbs a number of calculations into a single expression that is dependent upon source resistance and frequency. *NF* contour maps visually identify the optimal operating region, the area inside the 3dB contour. Although a figure of merit to compare different systems, there are other uses: one can derive RTI, source (sensor), and intrinsic noises, quantify SNR loss, determine noise-matched conditions, state the range of R_g in which $NF \leq 3$dB, and relate it to temperatures other than ambient. The latter was plotted as a sensor temperature vs. sensor resistance NF contour map where the optimal performance was the region above the 3dB line. Throughout this work, there was composite dependence of F_{min} on R_L, which implied that lower F values (and higher R_n) follow higher R_L values.

Dc blocking issues were also examined. An improper d.c. blocking capacitor value selection could place a resonant peak at or near a region of interest altering the measurement. It was shown that the effect on the *NF* reshaped the contours such that there was more intrinsic noise at lower frequencies. Conclusion: if a dc-blocking capacitor is needed, choose a reasonably large value.

We concluded by reducing the multi-element gain system to a single element. Generalizing the power gain with the unloaded transfer function and the ratio of input/output resistances, an indexed power gain formula for each element was generated. The product of these separate power gains gave the system power gain. Each element's intrinsic noise power was also used to derive the system's noise power and noise factor, F_{sys}. The optimal F_{sys} is one in which the power gain of the first device far exceeds the following devices. Knowledge of F_{sys} provides a system noise and SNR_{out} expression, a system r.m.s. noise expression that dictates the minimum signal voltage, and the system RTI and intrinsic noise spectral densities. From the latter two, an equation was introduced that converts and corrects data from the low-noise transformer-driven system to give sensor noise without having to contend with complex values.

Acknowledgements

The authors are most grateful to Dr. John Brasunas and Dr. Brook Lakew of NASA-GSFC for many hours of fruitful discussion.

References

[1] Nilsson J W 1993 *Electric Circuits* 4th edn (Reading, MA:Addison-Wesley Publishing Company, Inc.)
[2] Chen Wai-Kai 1991 *Active Network Analysis* (Singapore:World Scientific Publishing Co. Pte. Ltd.)
[3] Motchenbacher C D and Connelly J A 1993 *Low-Noise Electronic System Design* (NY: John Wiley & Sons, Inc.)
[4] EG&G PARC model 1900 literature 2002 *Model 1900 Precision Low-Noise Signal Transformer Instruction Manual* (Ametek Advanced Measurement Technology, Inc.)
[5] Johnson, J B 1928 Thermal agitation of electricity in conductors *Phys. Rev.* **32** 97-107
[6] Nyquist H 1928 Thermal agitation of electric charge in conductors *Phys. Rev.* **32** 110-3
[7] Letzter S and Webster N 1970 Noise in amplifiers *IEEE Spectrum* 67-75
[8] Fish P J 1994 *Noise and Low Noise Design* (NY: McGraw-Hill Inc.)
[9] Blinchikoff H J and Zverev A I 1976 *Filtering in the Time and Frequency Domains* (NY:John Wiley & Sons, Inc.)
[10] Haus H A *et al* 1960 Representation of noise in linear two-ports *Proceeding of the IRE* **32** 69-74
[11] Haus H A *et al* 1960 IRE standards on methods of measuring noise in linear two-ports, 1959 *Proceeding of the IRE* **32** 60-68
[12] Netzer, Y 1981 The design of low-noise amplifiers *Proceedings of the IEEE* **69** 728-741
[13] Friis H T 1944 Noise figures of radio receivers *Proceeding of the IRE*, **32** 419-421
[14] Horowitz P and Hill W 1989 *The Art of Electronics, 2nd Ed*., (NY: Cambridge University Press) p 22

Figure 1:

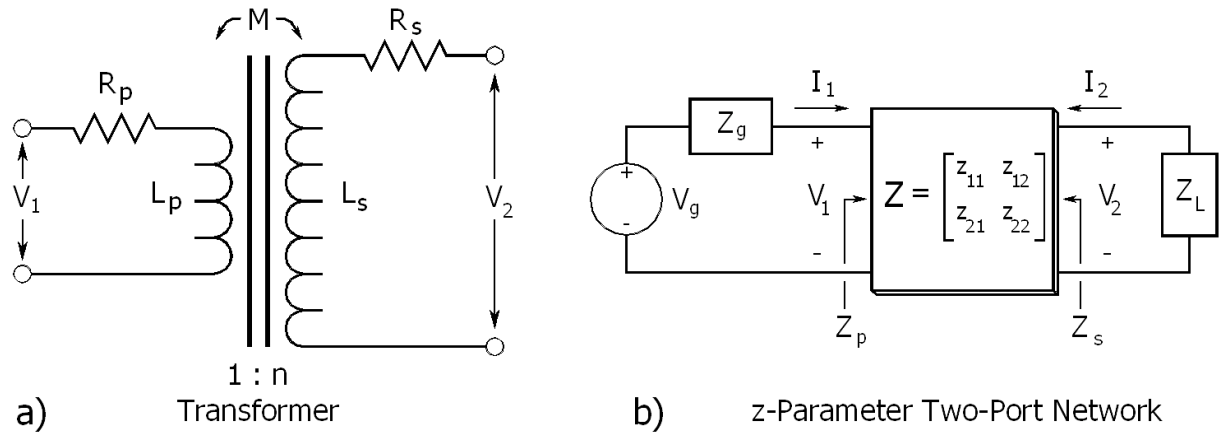

Figure 1. Schematic diagrams of (*a*) transformer and (*b*) the two-port *z*-parameter network of the transformer.

Figure 2:

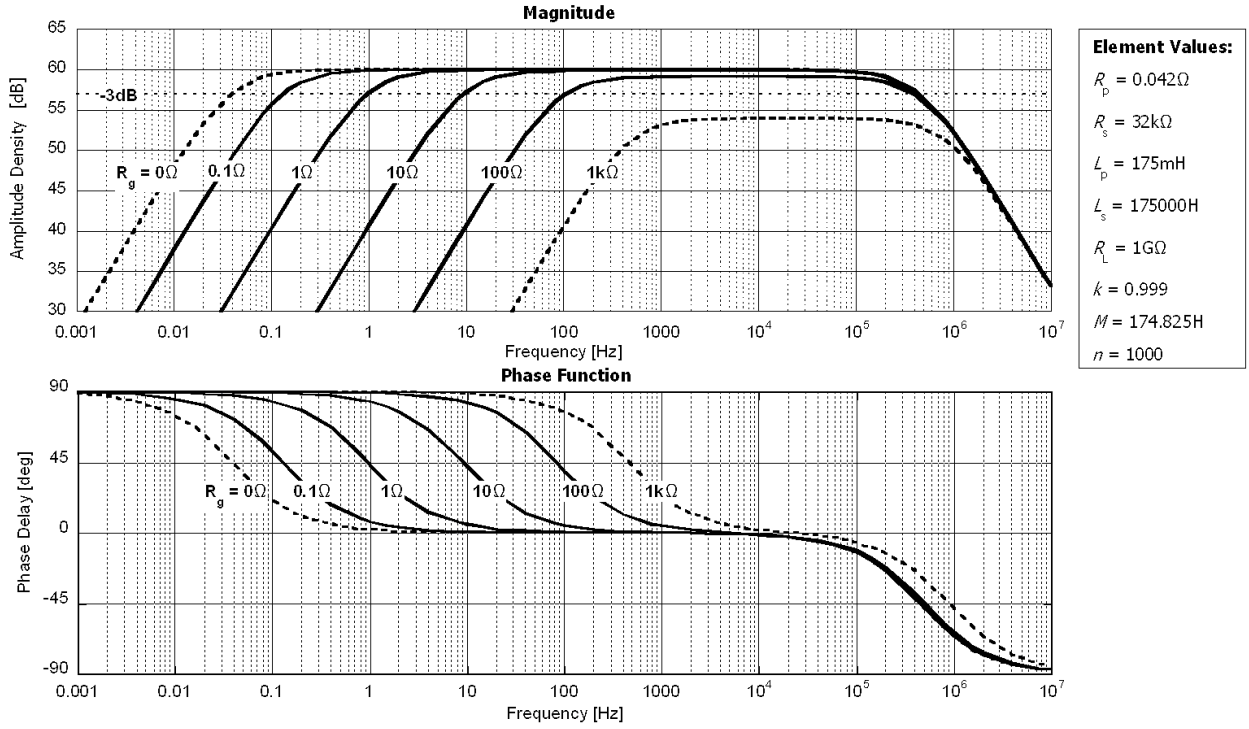

Figure 2. Family of 2nd-order approximations of (*a*) magnitude and (*b*) phase function, both functions of R_g and *f* for 1:1000 turns ratio, low-noise transformer using the inset element values as model parameters.

Figure 3:

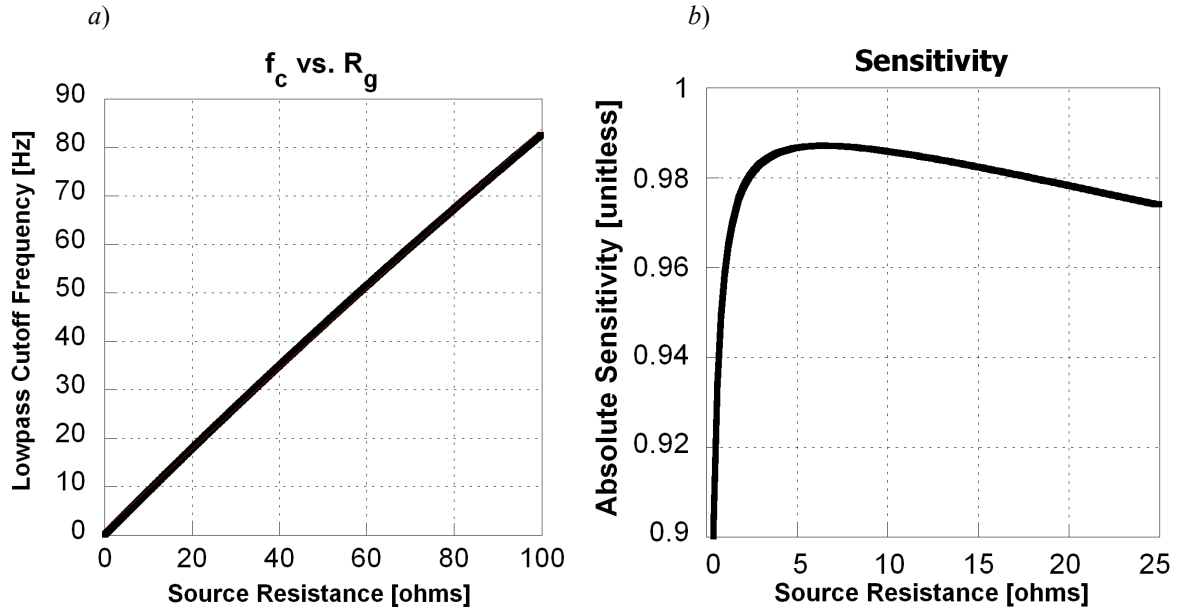

Figure 3. (*a*) Change in f_L with R_g and (*b*) sensitivity of f_L to R_g, both based on the model parameters.

Figure 4:

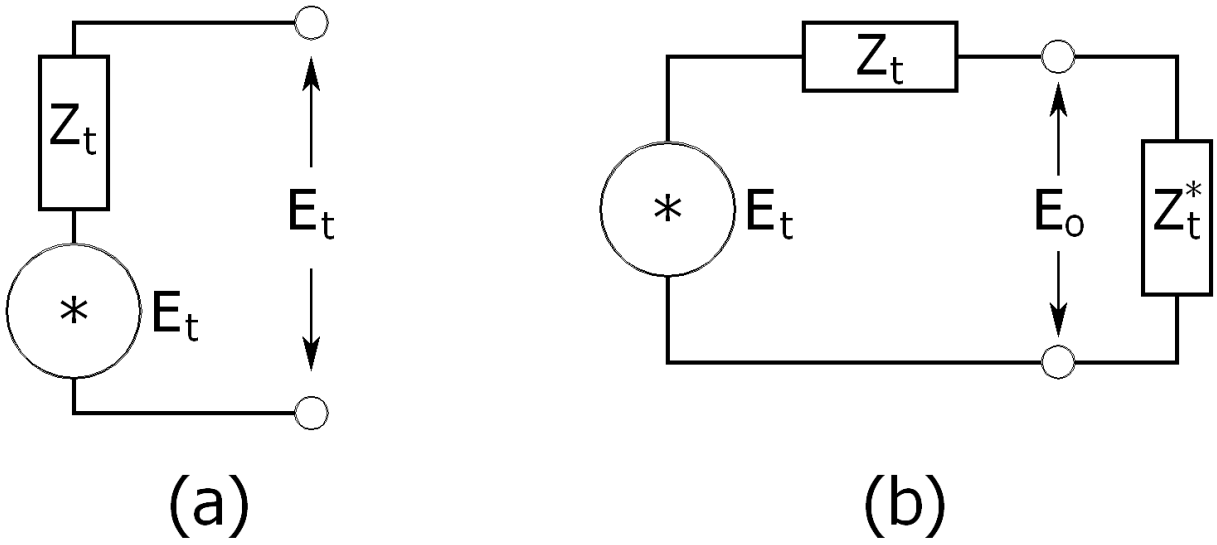

Figure 4. (*a*) Johnson noise voltage source circuit and (*b*) conjugate-matched closed circuit to measure Johnson noise voltage.

Figure 5:

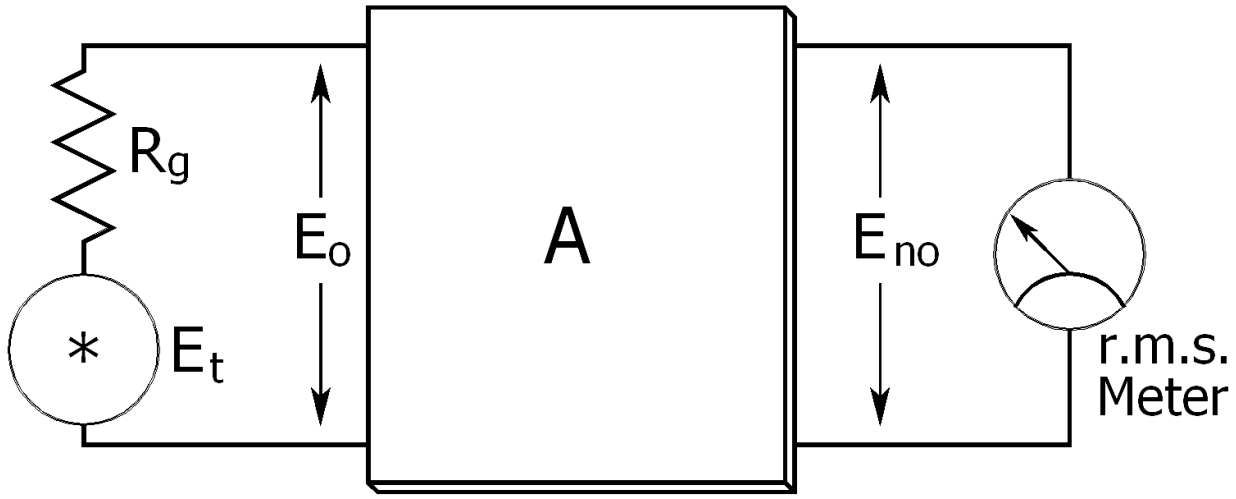

Figure 5. Source noise voltage generator applied to network with output connected to true-r.m.s. meter.

Figure 6:

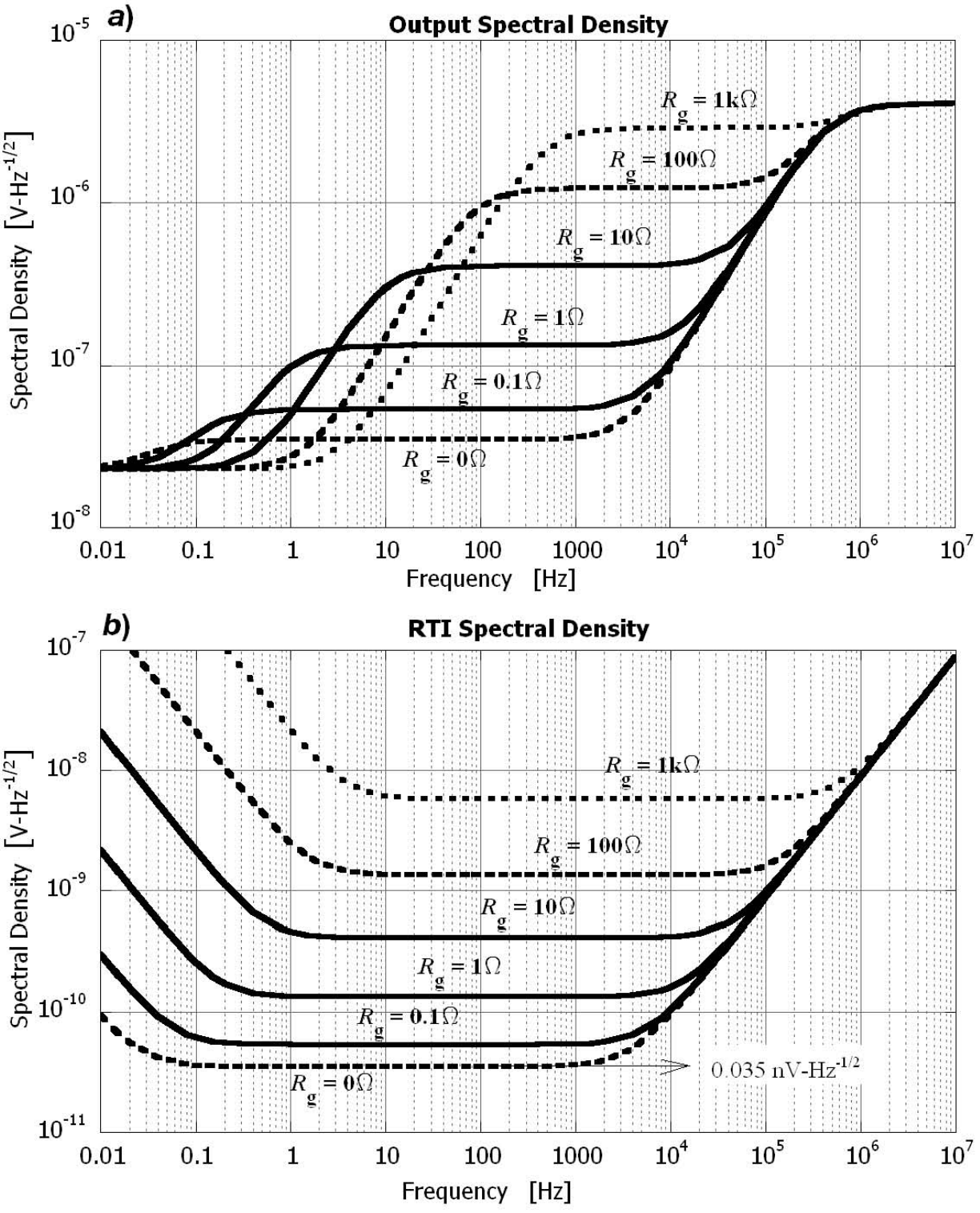

Figure 6. Family of spectral density curves for (*a*) output noise voltage and (*b*) RTI noise voltage using the model parameters.

Figure 7:

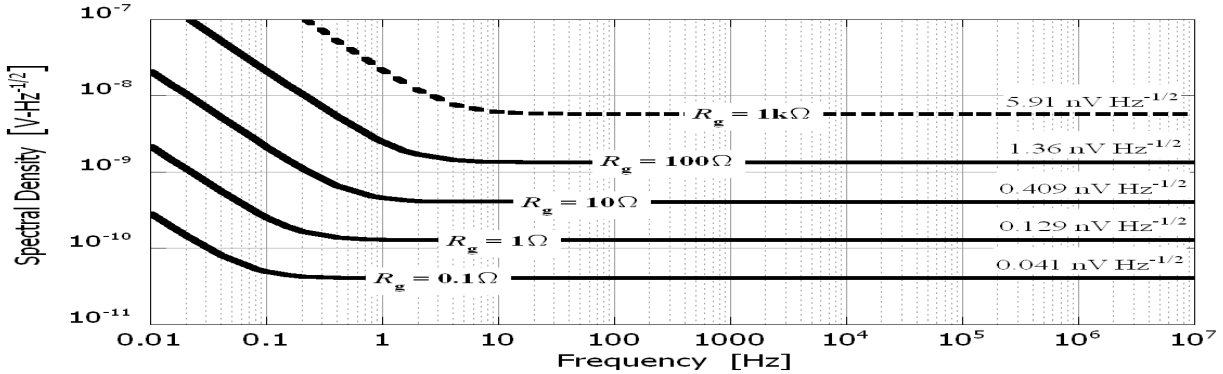

Figure 7. Family of spectral density correction curves based on subtracting in quadrature the baseline RTI noise. However, the input source thermal noise is not accurately reflected. Used the model parameters.

Figure 8:

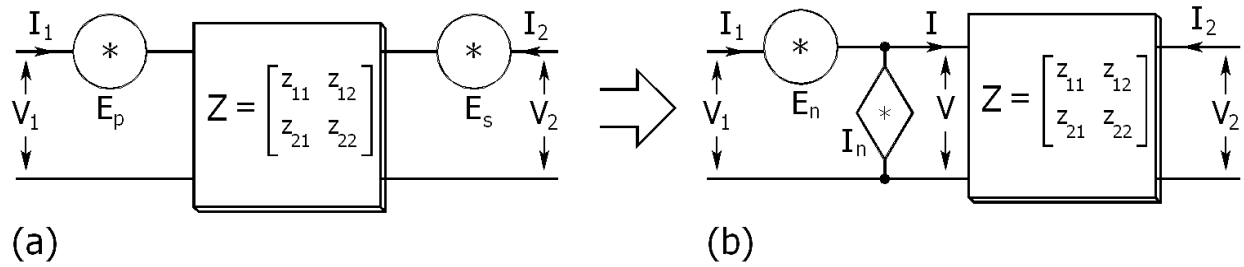

Figure 8. (*a*) Two port noiseless network with extracted noise voltage sources place at each port and (*b*) equivalent two port noiseless network with noise voltage/current sources placed the (primary) input.

Figure 9:

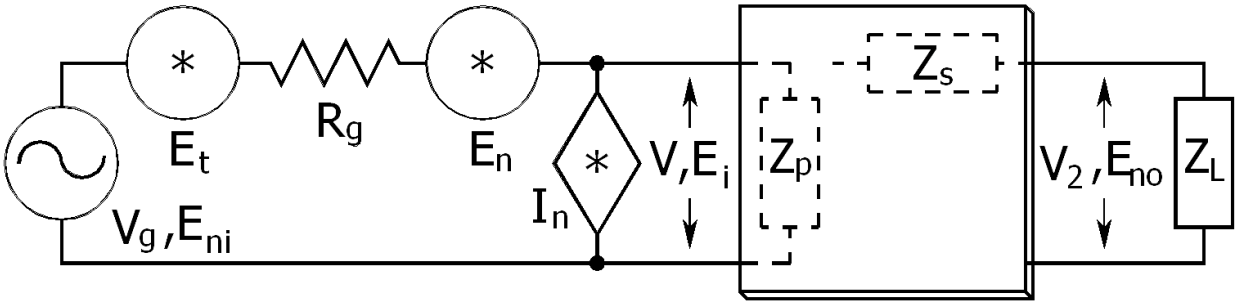

Figure 9. Equivalent noise sources E_n and I_n with input signal and noise source V_g and E_t.

Figure 10:

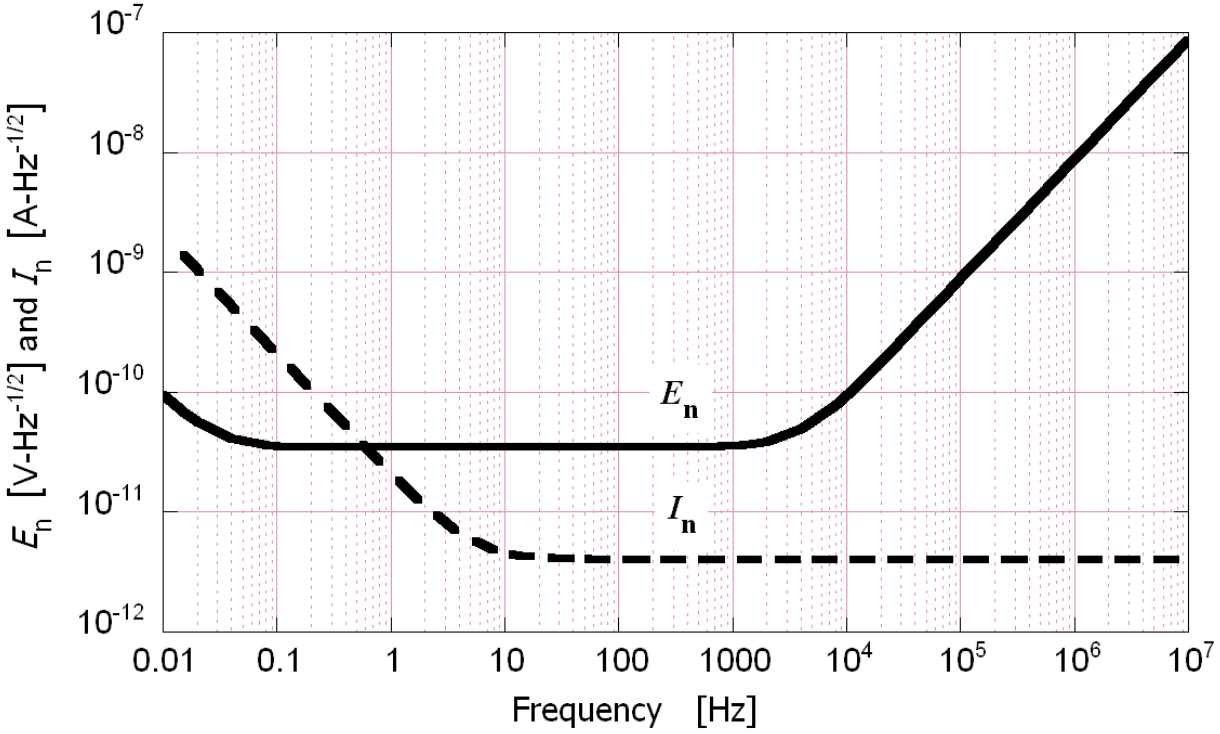

Figure 10. Equivalent noise voltage, E_n, and current, I_n, spectral densities based on model parameters.

Figure 11:

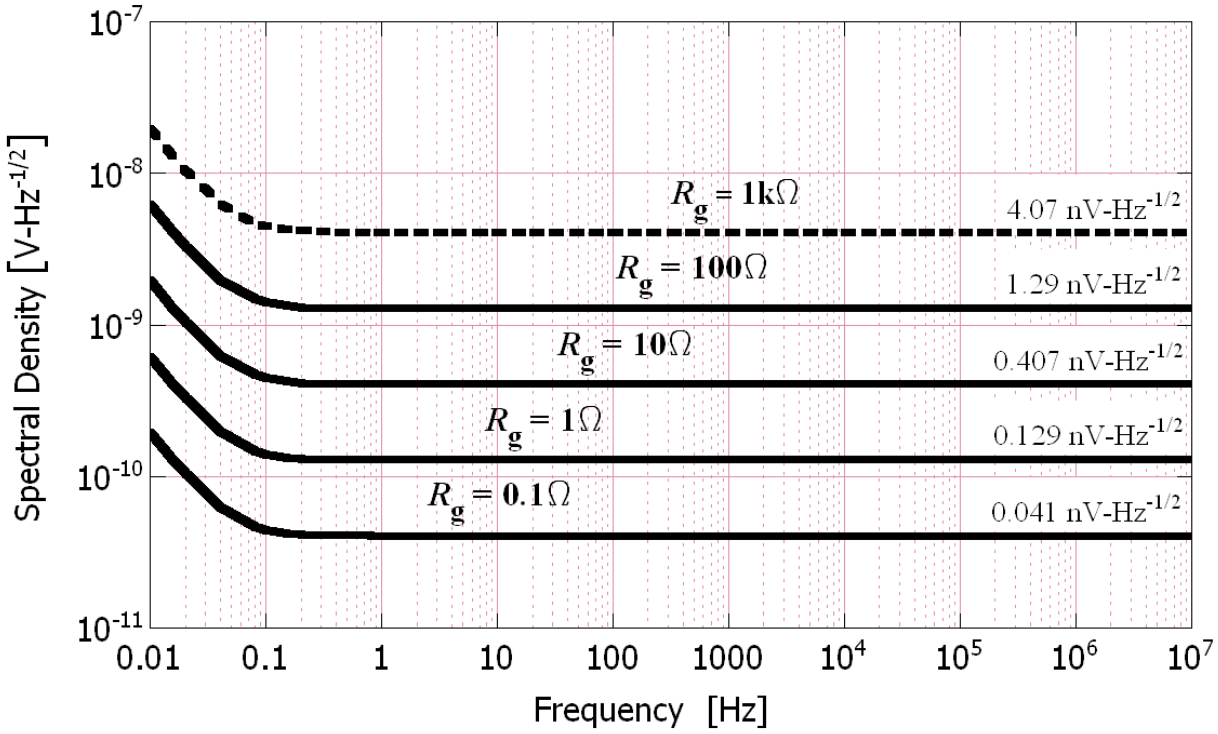

Figure 11. RTI spectral density, S_{ni}, corrected with S_{En} and S_{In} to give true source resistance noise, S_t.

Figure 12:

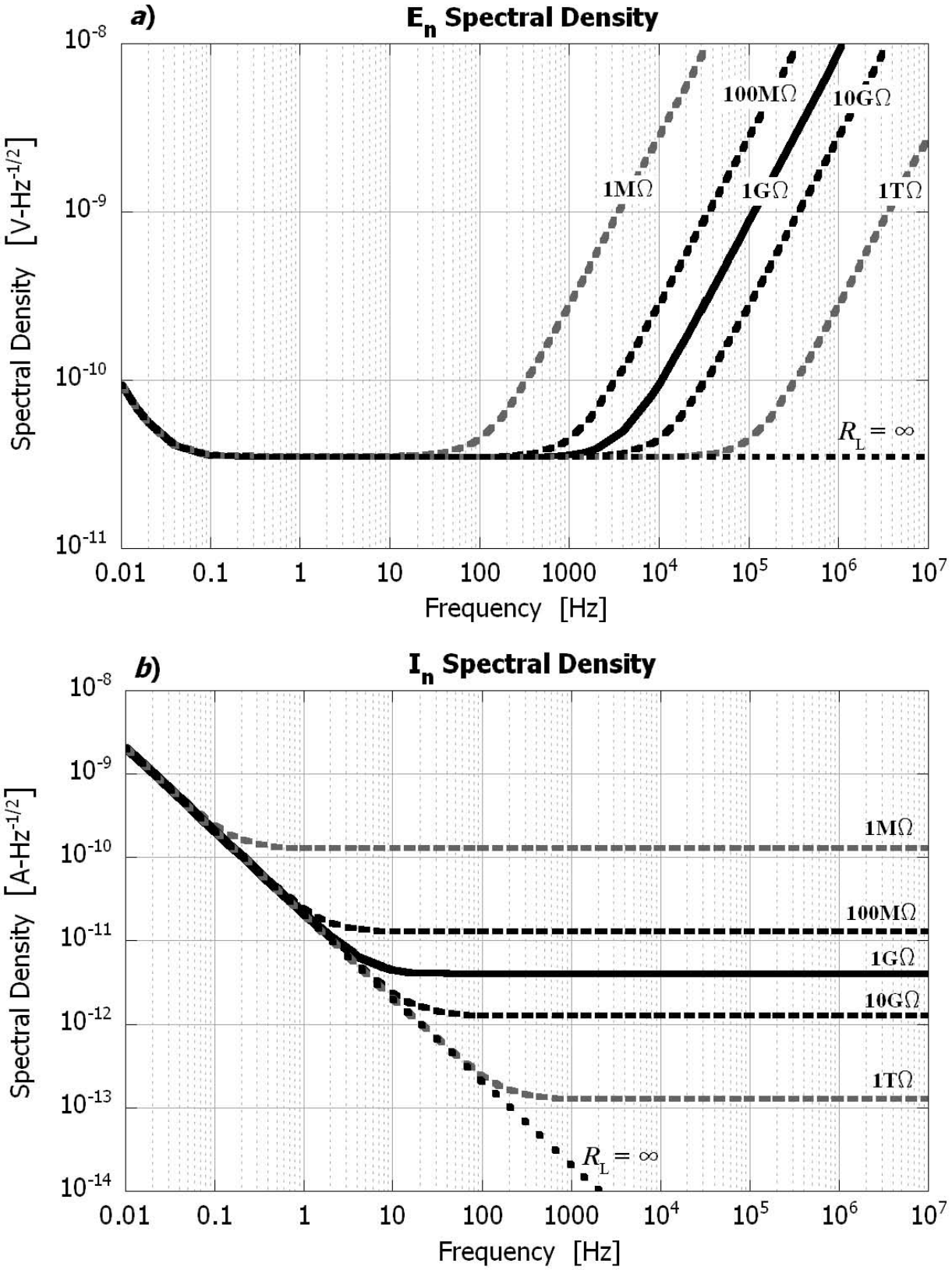

Figure 12. Examples of spectral densities from noise source generators (a) E_n and (b) I_n, both as functions of load resistance R_L**.** Results based on model parameters.

Figure 13:

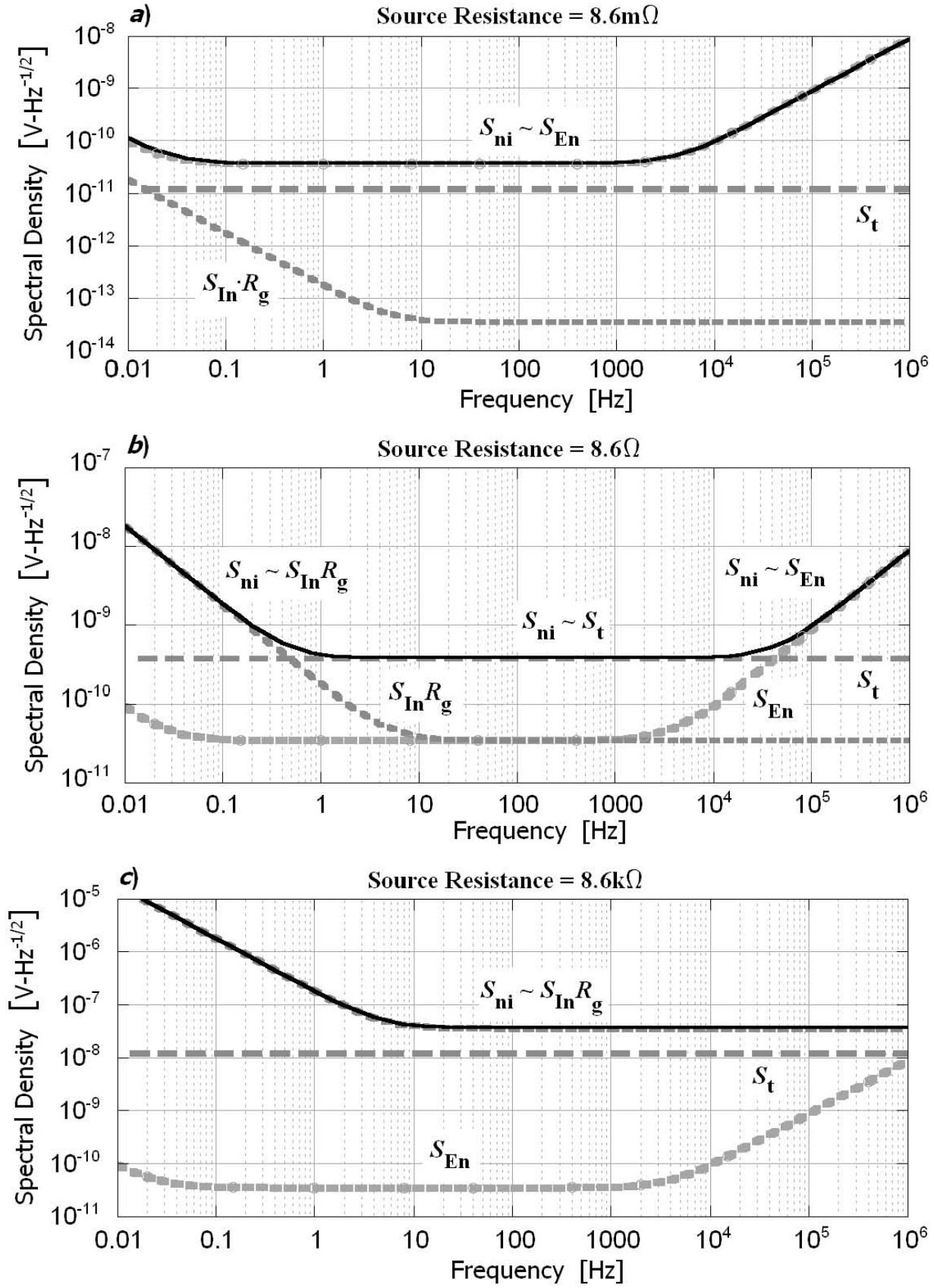

Figure 13. S_{ni}, S_t, S_{En}, and $S_{In}{\cdot}R_g$ vs R_g at (*a*) 8.6mΩ, (*b*) 8.6Ω, and (*c*) 8.6kΩ using the model parameters.

Figure 14:

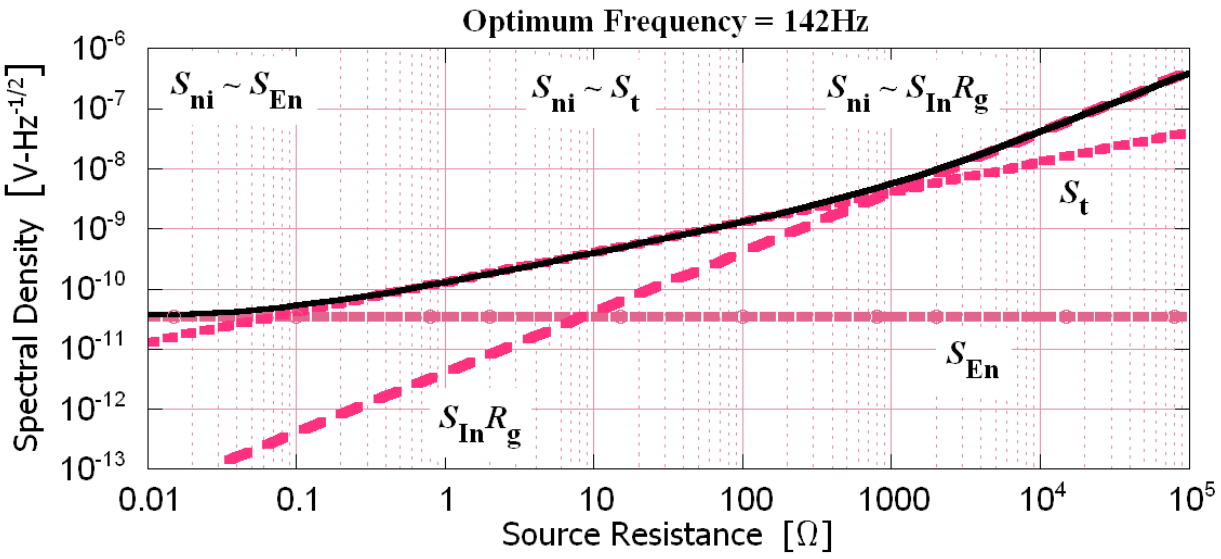

Figure 14. S_{ni}, S_t, S_{En}, and $S_{In}{\cdot}R_g$ vs R_g at optimum frequency 142Hz using the model parameters.

Figure 15:

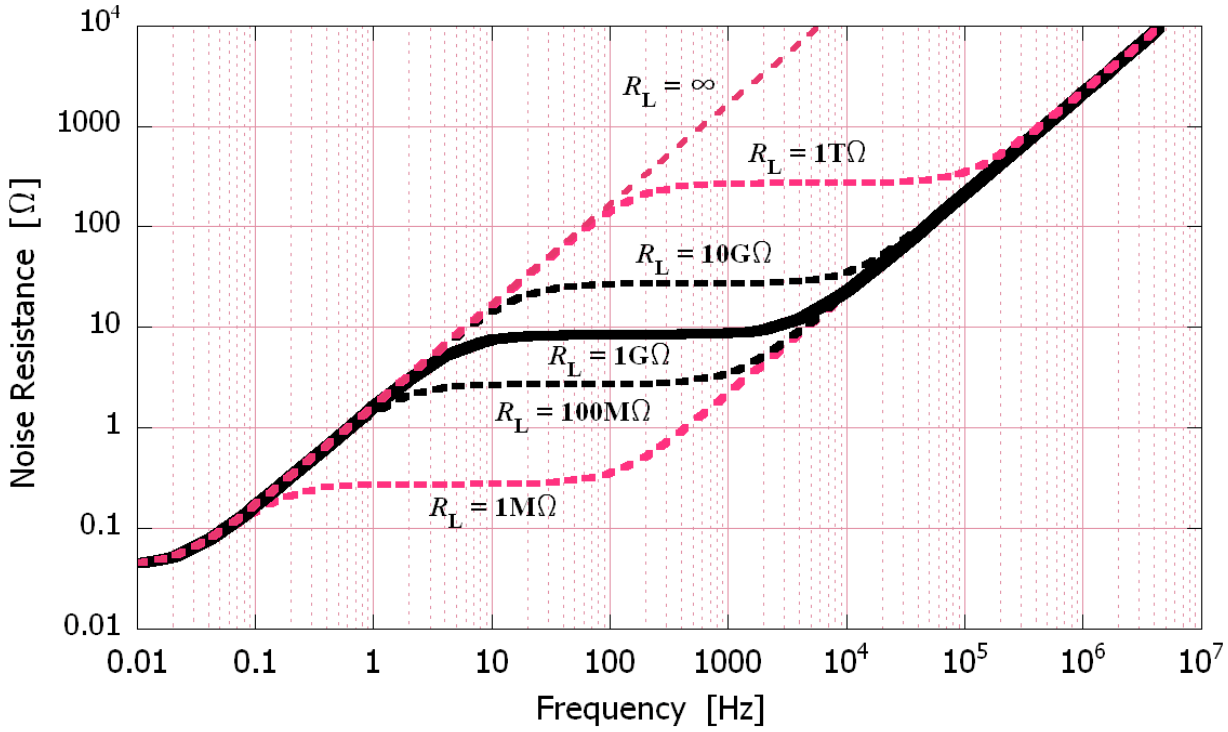

Figure 15. Noise resistance, R_n, mapped at various load resistances, R_L, using the model parameters.

Figure 16:

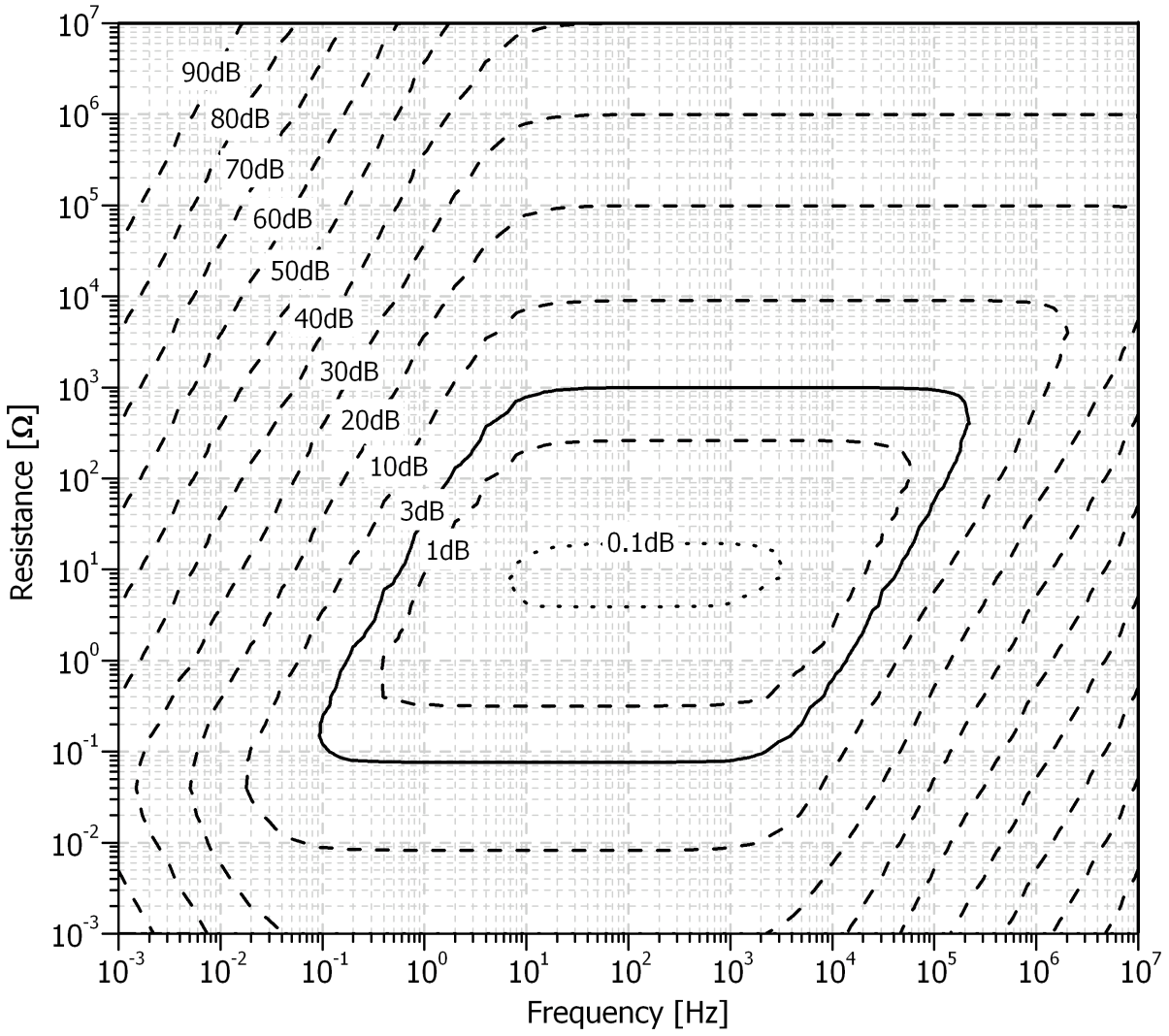

Figure 16. Example low noise transformer NF contour map with turns-ratio n = 1000 and load of R_L = 1GΩ. Based on model parameters of inset in figure 2.

Figure 17:

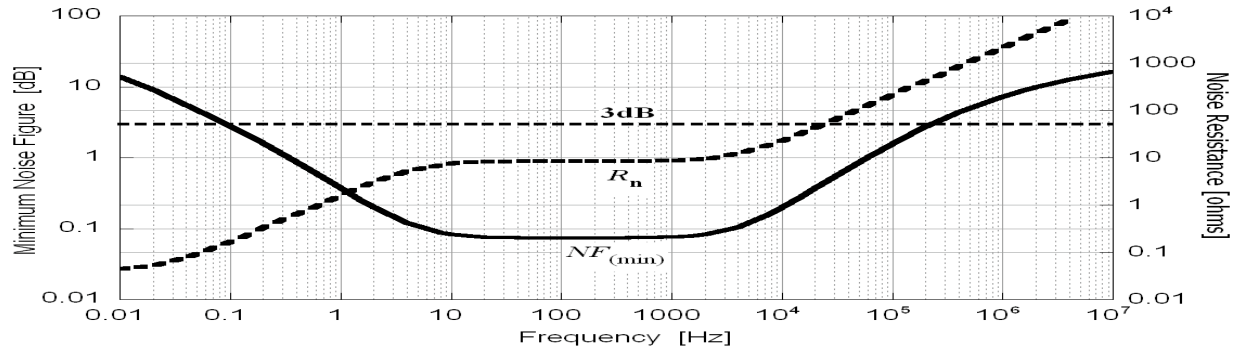

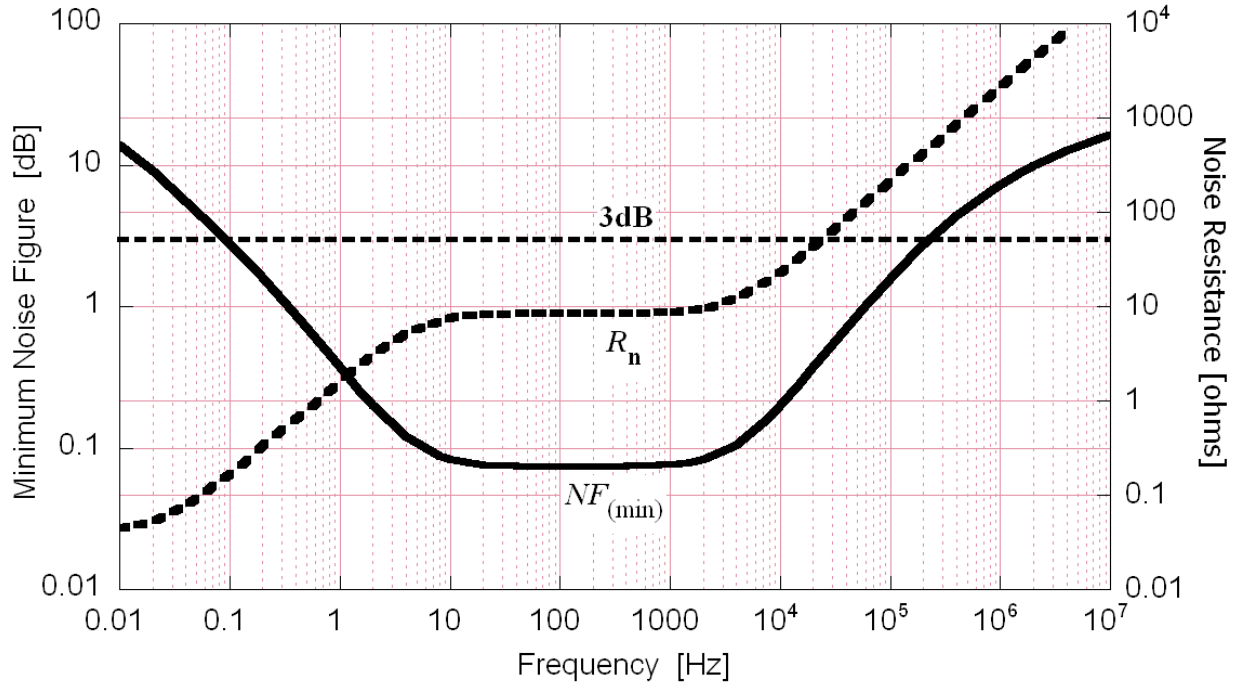

Figure 17. Mapping of $NF_{(min)}$, and R_n, for R_L = 1GΩ based the model parameters.

Figure 18:

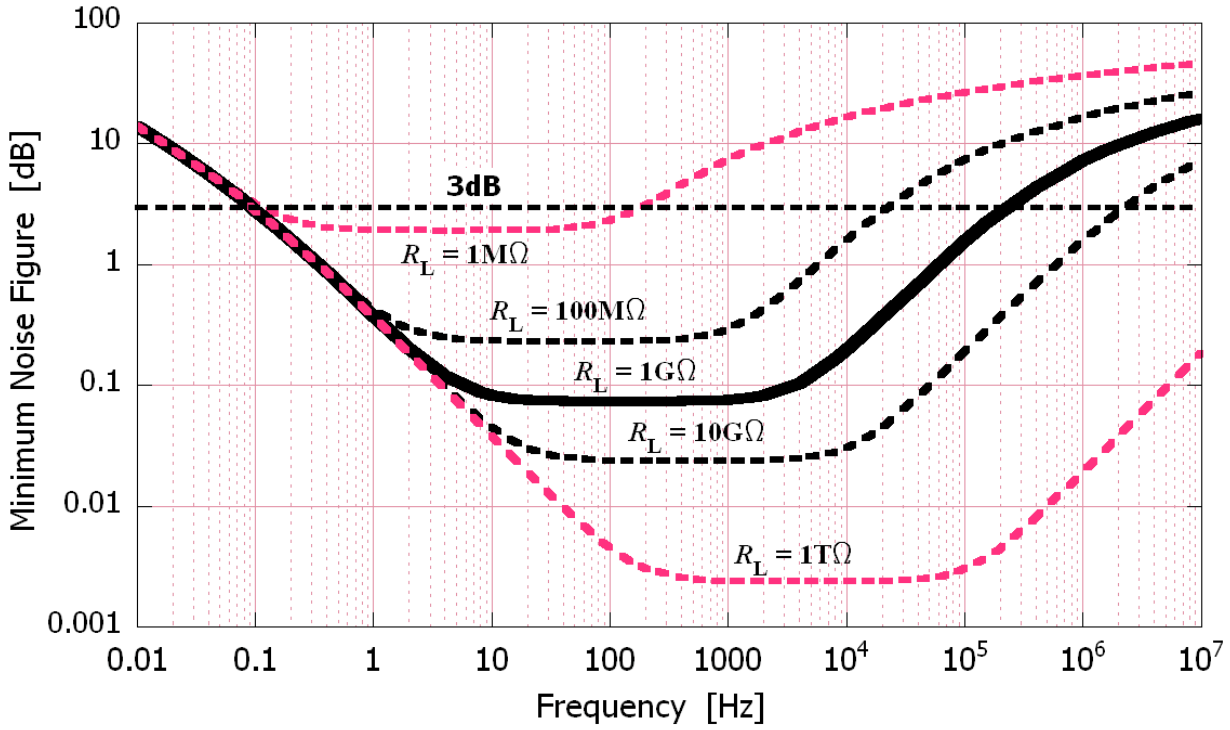

Figure 18. Mapping of minimum noise figure ($NF_{(min)}$) of transformer model using the model parameters at various load resistances (R_L) values.

Figure 19:

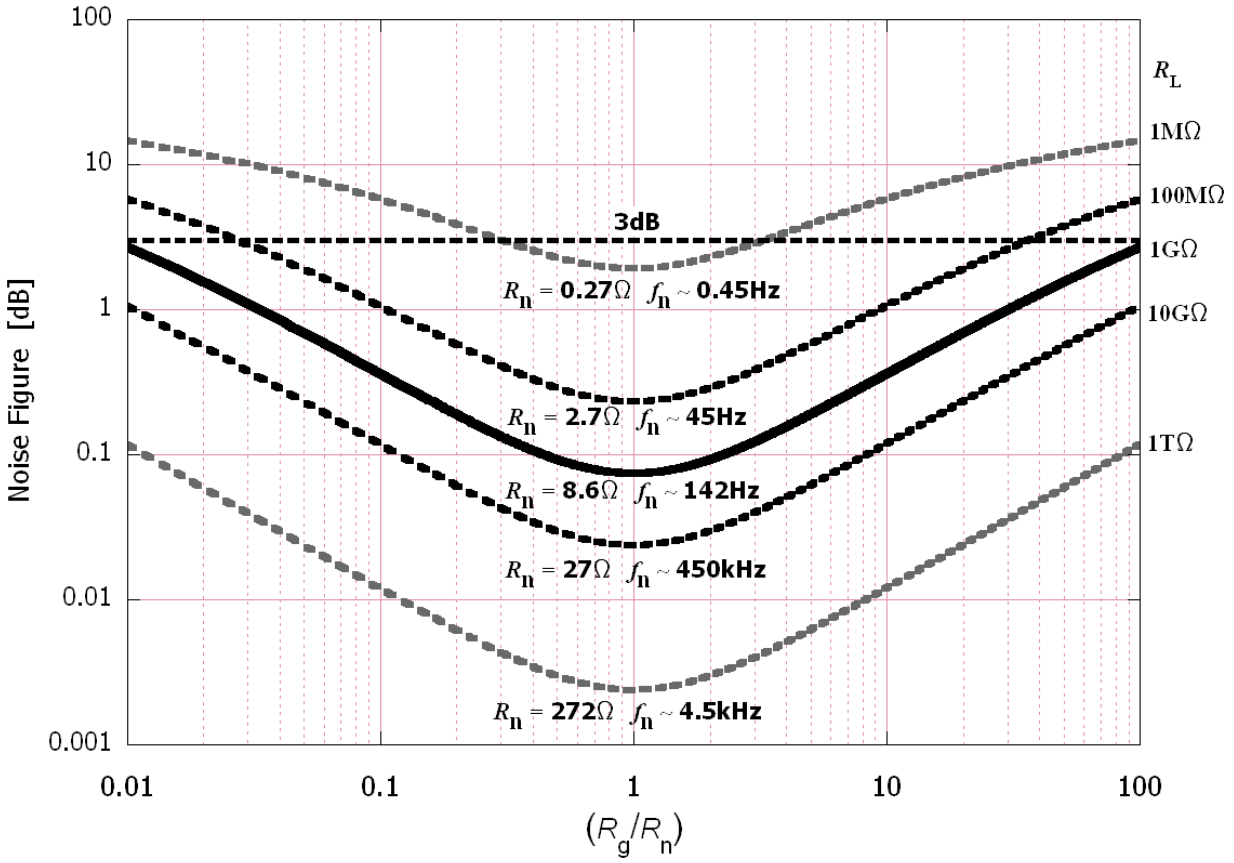

Figure 19. Noise figure (*NF*) versus R_g/R_n of transformer model using the model parameters at various load resistance (R_L) values.

Figure 20:

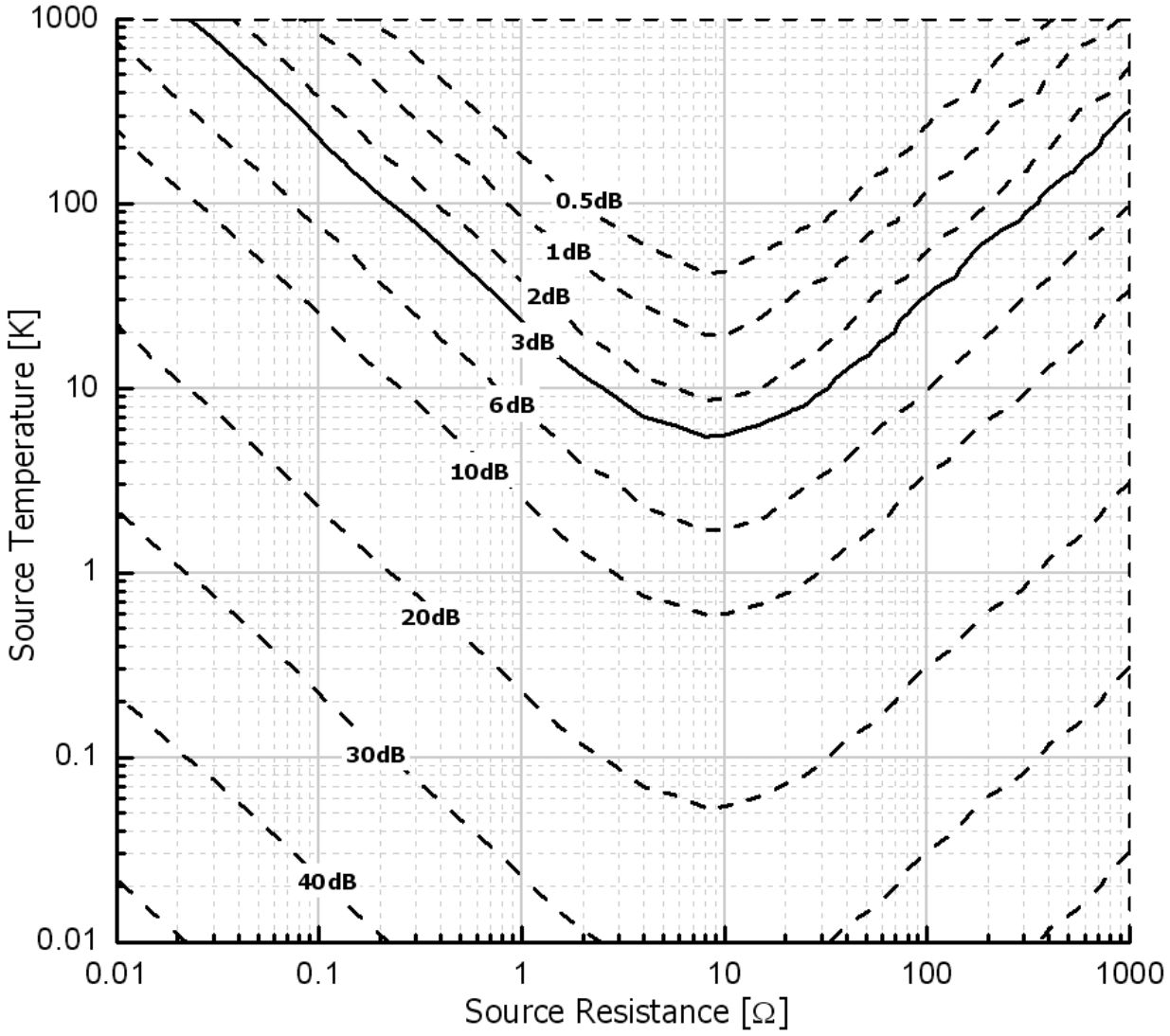

Figure 20. NF_x *vs.* R_g and source temperature T with transformer fixed at $T_a = 290$K and $R_L = 1G\Omega$.

Figure 21:

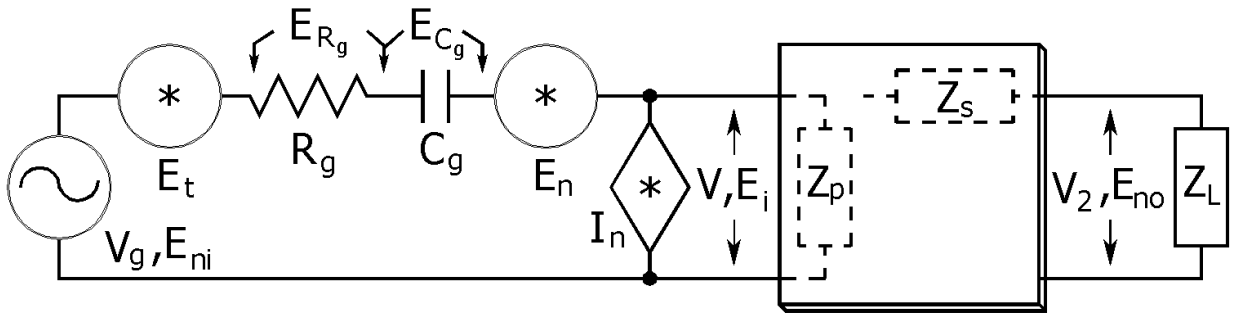

Figure 21. Equivalent input noise source circuit with capacitor in series (see figure 9).

Figure 22:

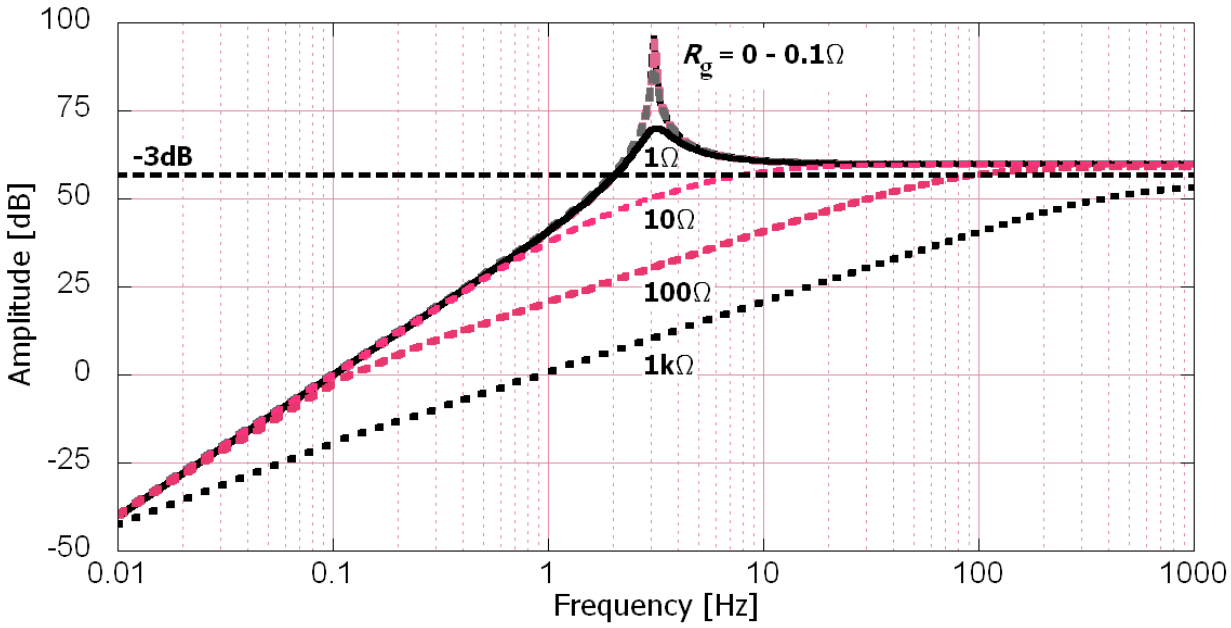

Figure 22. Amplitude density of transformer model with a 15mF dc-blocking capacitor at primary. Results based the model parameters of figure 2.

Figure 23:

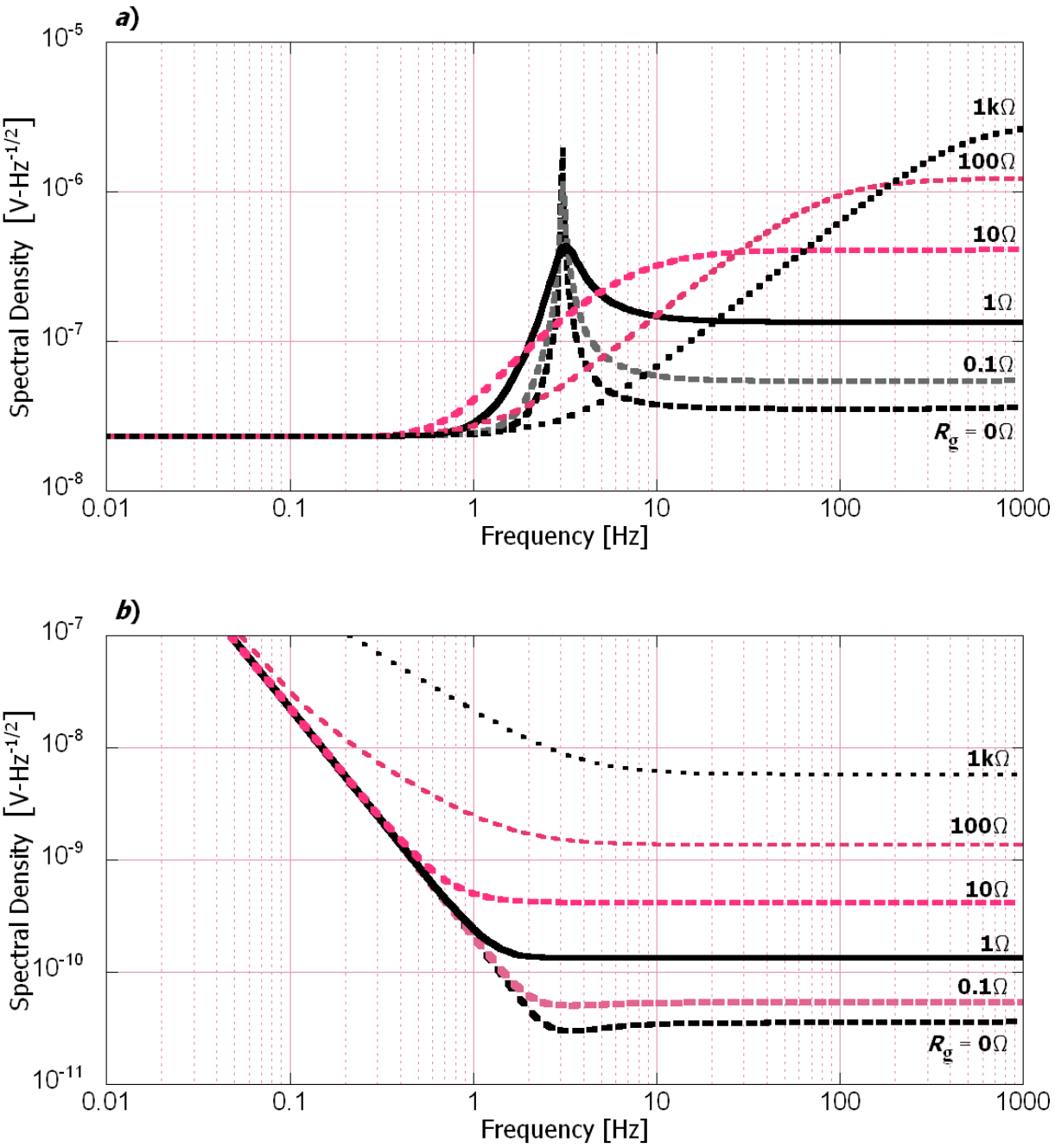

Figure 23. (a) Output and (b) input noise spectral densities of low noise transformer model with a 15mF dc-blocking capacitor at the transformer's primary terminals. Results based on the model parameters.

Figure 24:

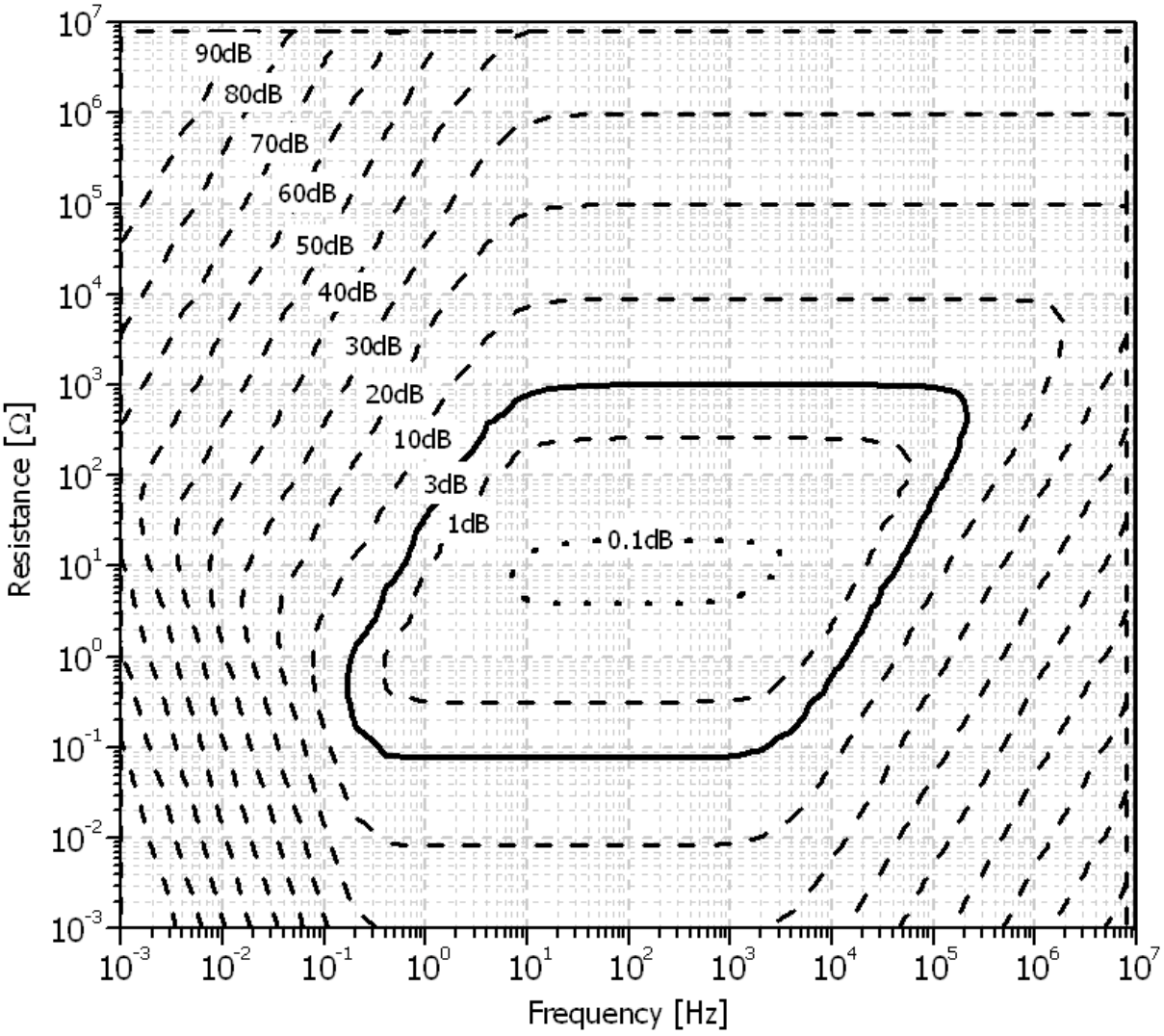

Figure 24. Noise figure contour map for $n = 1000$, low noise transformer model with dc block capacitance $C_g = 2.3$F and load resistance $R_L = 1$GΩ. Based on model parameters from inset in figure 2.

Figure 25:

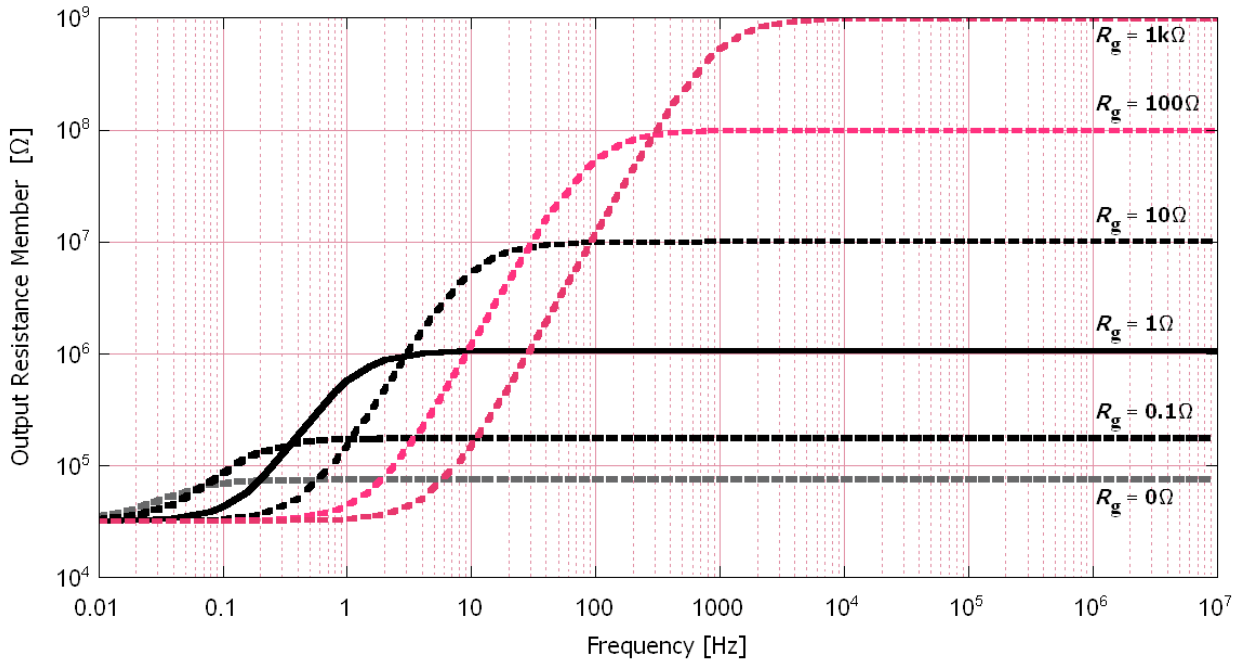

Figure 25. Resistance member (R_{os}) of the transformer output impedance using the model parameters.

Figure 26:

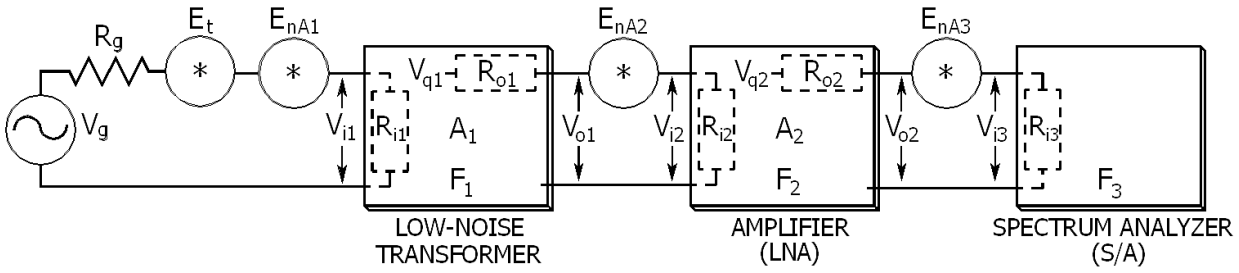

Figure 26. Measurement system of cascaded transformer, low noise amplifier, and spectrum analyzer networks with associated noise sources. LNA drive resistance is typically R_{o_2} = 50Ω or 600Ω

Figure 27:

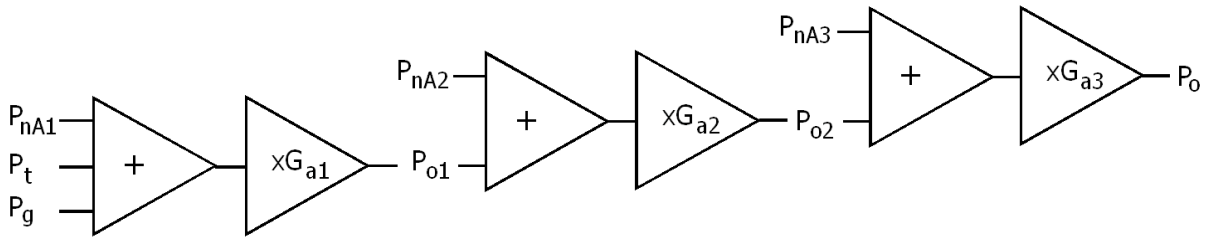

Figure 27. Sum-product block diagram of power transfer through a system network.

Figure 28:

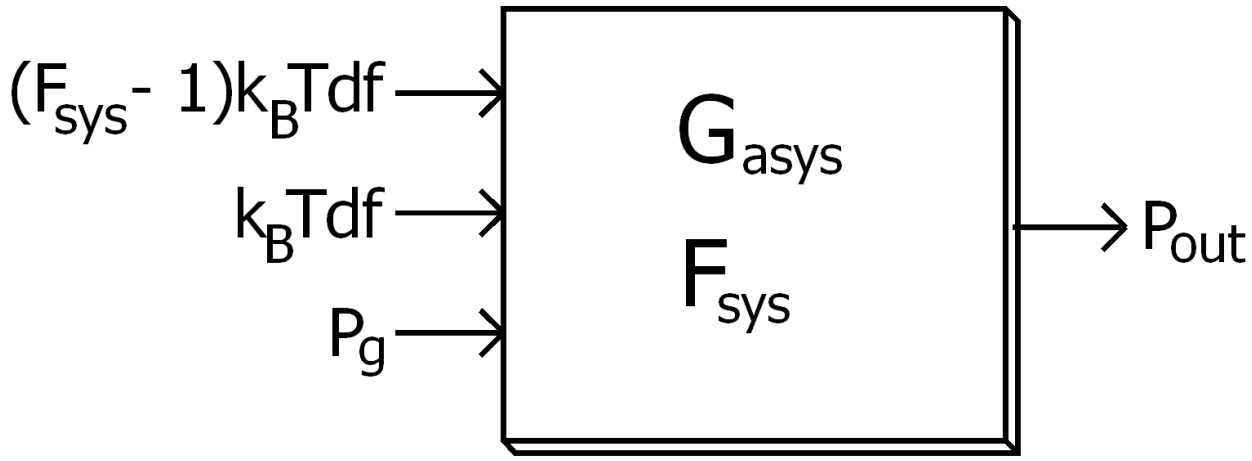

Figure 28. Block diagram of system network in terms of signal, source noise, and intrinsic noise powers.

Figure 29:

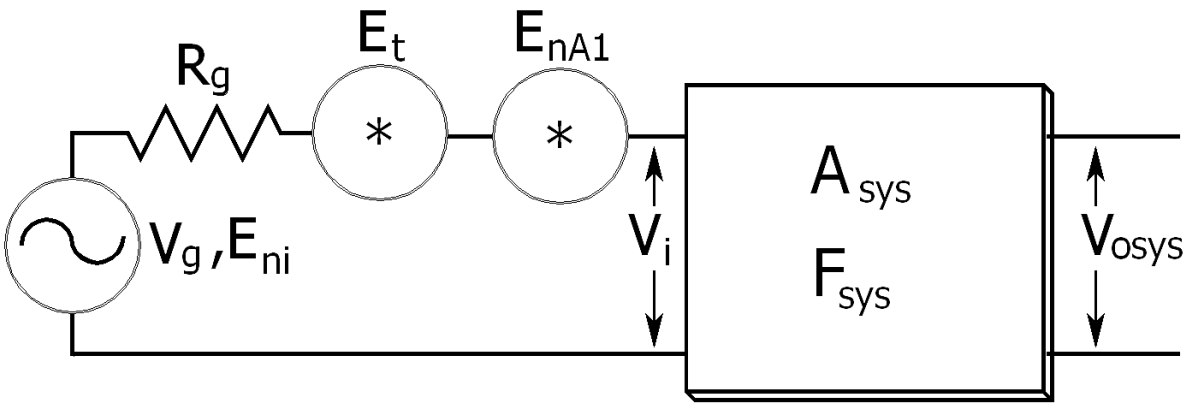

Figure 29. Diagram of a measurement system network in terms of signal- and noise-related voltages.

Table 1. Corrected RTI spectral densities vs. actual thermal noise spectral density, S_t, from figure 7.

R_g	S_v(100 Hz)	S_t	error (%)
0.1 Ω	0.0407 nV/√Hz	0.0407 nV/√Hz	0.012 %
1 Ω	0.1288 nV/√Hz	0.1287 nV/√Hz	0.058 %
10 Ω	0.4091 nV/√Hz	0.407 nV/√Hz	0.508 %
100 Ω	1.35 nV/√Hz	1.287 nV/√Hz	4.91 %
1 kΩ	5.763 nV/√Hz	4.070 nV/√Hz	41.6 %

Table 2:

Table 2. Noise factors and noise spectral densities for various R and T values at source generator temperature T_a = 290K and load resistance R_L = 1GΩ—the operating frequency is f = 100 Hz.

T	R_g	$F_{min\,x}$, [Eq. (73)]	F_x, [Eq. (72)]	S_t	$S_{ni\,x} = S_t\sqrt{F_x}$	$S_{A\,x} = S_t\sqrt{F_x - 1}$
T_a	30 Ω	1.017 (0.07dB)	1.032 (0.14dB)	0.693 nV/√Hz	0.704 nV/√Hz	0.125 nV/√Hz
77K	3 Ω	1.065 (0.27dB)	1.104 (0.43dB)	0.113 nV/√Hz	0.119 nV/√Hz	0.0365 nV/√Hz
40K	0.3 Ω	1.125 (0.51dB)	2.791 (4.46dB)	0.026 nV/√Hz	0.043 nV/√Hz	0.034 nV/√Hz